The noncoding RNA CcnA modulates the master cell cycle regulators CtrA and GcrA in Caulobacter crescentus

Wanassa Beroual, Karine Prévost, David Lalaouna, Nadia Ben Zaina, Odile Valette, Yann Denis, Meriem Djendli, Gaël Brasseur, Matteo Brilli, Marta Robledo Garrido, et al.

PLOS BIOLOGY

RESEARCH ARTICLE

The noncoding RNA CcnA modulates the master cell cycle regulators CtrA and GcrA in *Caulobacter crescentus*

Wanassa Beroual[1], Karine Prévost[2], David Lalaouna[2¤a], Nadia Ben Zaina[1], Odile Valette[1], Yann Denis[3], Meriem Djendli[1], Gaël Brasseur[1], Matteo Brilli[4], Marta Robledo Garrido[5], Jose-Ignacio Jimenez-Zurdo[5], Eric Massé[2], Emanuele G. Biondi[1¤b]*

1 Aix-Marseille Université, CNRS, LCB, IMM, Turing Center for Living Systems, Marseille, France, **2** Département de biochimie et de génomique fonctionnelle, RNA Group, Université de Sherbrooke, Sherbrooke, Quebec, Canada, **3** Aix-Marseille Univ, CNRS, Plate-forme Transcriptome, IMM, Marseille, France, **4** Pediatric Clinical Research Center "Romeo ed Enrica Invernizzi", Department of Biosciences, University of Milan, Milan, Italy, **5** Grupo de Ecología Genética de la Rizosfera, Estación Experimental del Zaidín, Consejo Superior de Investigaciones Científicas (CSIC), Granada, Spain

¤a Current address: Université de Strasbourg, CNRS, ARN UPR 9002, Strasbourg, France
¤b Current address: Université Paris-Saclay, CEA, CNRS, Institute for Integrative Biology of the Cell (I2BC), Gif-sur-Yvette, France
* emanuele.biondi@i2bc.paris-saclay.fr

OPEN ACCESS

Citation: Beroual W, Prévost K, Lalaouna D, Ben Zaina N, Valette O, Denis Y, et al. (2022) The noncoding RNA CcnA modulates the master cell cycle regulators CtrA and GcrA in *Caulobacter crescentus*. PLoS Biol 20(2): e3001528. https://doi.org/10.1371/journal.pbio.3001528

Academic Editor: Matthew K. Waldor, Brigham and Women's Hospital, UNITED STATES

Received: July 22, 2020

Accepted: January 5, 2022

Published: February 22, 2022

Data Availability Statement: All fastQ files are available from the Dryad database (doi:10.5061/dryad.4mw6m909k).

Funding: This research was funded by the Agence Nationale Recherche (ANR; ANR-17-CE20-0011-01) to EGB. The funders had no role in study design, data collection and analysis, decision to publish, or preparation of the manuscript.

Competing interests: The authors have declared that no competing interests exist.

Abstract

Bacteria are powerful models for understanding how cells divide and accomplish global regulatory programs. In *Caulobacter crescentus*, a cascade of essential master regulators supervises the correct and sequential activation of DNA replication, cell division, and development of different cell types. Among them, the response regulator CtrA plays a crucial role coordinating all those functions. Here, for the first time, we describe the role of a novel factor named CcnA (cell cycle noncoding RNA A), a cell cycle–regulated noncoding RNA (ncRNA) located at the origin of replication, presumably activated by CtrA, and responsible for the accumulation of CtrA itself. In addition, CcnA may be also involved in the inhibition of translation of the S-phase regulator, GcrA, by interacting with its 5′ untranslated region (5′ UTR). Performing in vitro experiments and mutagenesis, we propose a mechanism of action of CcnA based on liberation (*ctrA*) or sequestration (*gcrA*) of their ribosome-binding site (RBS). Finally, its role may be conserved in other alphaproteobacterial species, such as *Sinorhizobium meliloti*, representing indeed a potentially conserved process modulating cell cycle in *Caulobacterales* and *Rhizobiales*.

Introduction

Caulobacter crescentus is a pivotal model organism to understand how basic functions of the cell physiology are organized and coordinated through the cell cycle [1,2] (Fig 1A). *C. crescentus* combines the cultivation and genetic simplicity of a prokaryotic system with a regulatory intricacy that is a paradigm of global regulatory programs of all living organisms.

Abbreviations: CcnA, cell cycle noncoding RNA A; CcnA, as, antisense of CcnA; DEG, differentially expressed gene; LB, lysogeny broth; MAPS, MS2-affinity purification coupled with RNA sequencing; ncRNA, noncoding RNA; PYE, peptone yeast extract; qRT-PCR, quantitative real-time PCR; RBS, ribosome-binding site; RNAseq, RNA sequencing; RPKM, reads per kilobase per million mapped reads; SD, Shine–Dalgarno; TSS, transcriptional start site; TY, tryptone-yeast; WT, wild-type; 5′ UTR, 5′ untranslated region.

Transcriptional regulation plays a major role during cell cycle progression. Several master regulators controlling transcription (i.e., DnaA, GcrA, CcrM, and CtrA) are sequentially activated in order to induce transcription of hundreds of genes required at specific phases of the cycle [3–5]. Each phase is under the control of the following well-defined factors: (i) the initiation of the S-phase depends on DnaA; (ii) the first part of the S-phase depends on the epigenetic module GcrA and CcrM; and (iii) the second part depends on CtrA, which is also the regulator of the G1 phase of swarmer cells [6].

Other regulators of transcription intervene to fine-tune the cell cycle–regulated transcription of genes that must be activated at specific phases of the cell cycle; for example, MucR and SciP regulate CtrA activity [7–10]. The interconnections between DnaA, GcrA, CcrM, and CtrA create an intricate network whose behavior emerges from the integration of multiple master regulatory inputs. In particular, regulation of the essential response regulator CtrA is critical, as it directly or indirectly controls all the other master regulators of the cell cycle [11]. CtrA is notably responsible for the direct transcriptional activation of key genes for cell division and the biogenesis of polar structures (flagellum, stalk, and pili). CtrA also activates the transcription of the gene encoding the orphan adenine methyl transferase CcrM, which, in turn, is required for the regulation of many genes including the fine-tuned regulation of the promoter P1 of *ctrA* [5]. Moreover, CtrA indirectly blocks chromosome replication initiation promoted by DnaA by binding to sites in the origin of replication (*CORI*), resulting in DnaA exclusion from the *CORI* [12,13].

Another master regulator, named GcrA, activates the transcription of the *ctrA* gene, which, in turn, negatively feeds back on the transcription of *gcrA* [14–17]. GcrA activity is known to be affected by the methylation status of its targets' promoters. For instance, the GcrA-dependent transcription of *ctrA* from its P1 promoter is activated by the conversion of a CcrM-methylated site from its full to the hemi-methylation state approximately after a third of DNA replication [5]. P1 activation is, therefore, responsible for the first weak accumulation of CtrA and predates the activation of the stronger P2 promoter, located downstream of P1. P2 is under the control of phosphorylated CtrA (CtrA~P), responsible for the robust accumulation of CtrA in the second half of DNA replication. CtrA at its highest level is then responsible for the repression of its own P1 promoter and of *gcrA* transcription. Although the molecular details of this biphasic activation of *ctrA* are still only partially understood, the stronger activation of P2 may underscore other posttranscriptional mechanisms reinforcing CtrA accumulation.

Besides being finely regulated in time by the DnaA-GcrA-CcrM transcriptional cascade, activation of CtrA requires phosphorylation by the CckA-ChpT phosphorelay [18], which is linked to a sophisticated spatial regulation since the hybrid kinase CckA has a bipolar localization [18–20]. At the swarmer pole, CckA acts as a kinase due to the presence of the atypical kinase DivL and the DivK phosphatase PleC [9]. However, at the stalked pole, CckA is a phosphatase of CtrA because the kinase DivJ keeps the CtrA negative regulator DivK fully phosphorylated, turning the CckA-ChpT phosphorelay into a CtrA phosphatase. As CtrA~P blocks the origin of replication, a complex degradation machinery ensures its cell cycle–dependent degradation at the G1 to S-phase transition and after cell division in the stalk compartment. A cascade of adapter proteins (CpdR, RcdA, and PopA) is responsible for the specific and highly regulated proteolysis of CtrA [21,22].

Few cases of regulation of gene expression by ncRNAs have been characterized in *C. crescentus*. For example, the SsrA noncoding RNA (ncRNA) (tmRNA) is a small RNA associated to selected translating ribosomes to target the translated polypeptides for degradation. The tmRNA has been linked to replication control in *C. crescentus* [23] and *Escherichia coli* [24]. More generally, only 27 ncRNAs were described in *C. crescentus* [25]. Among them, CrfA is a

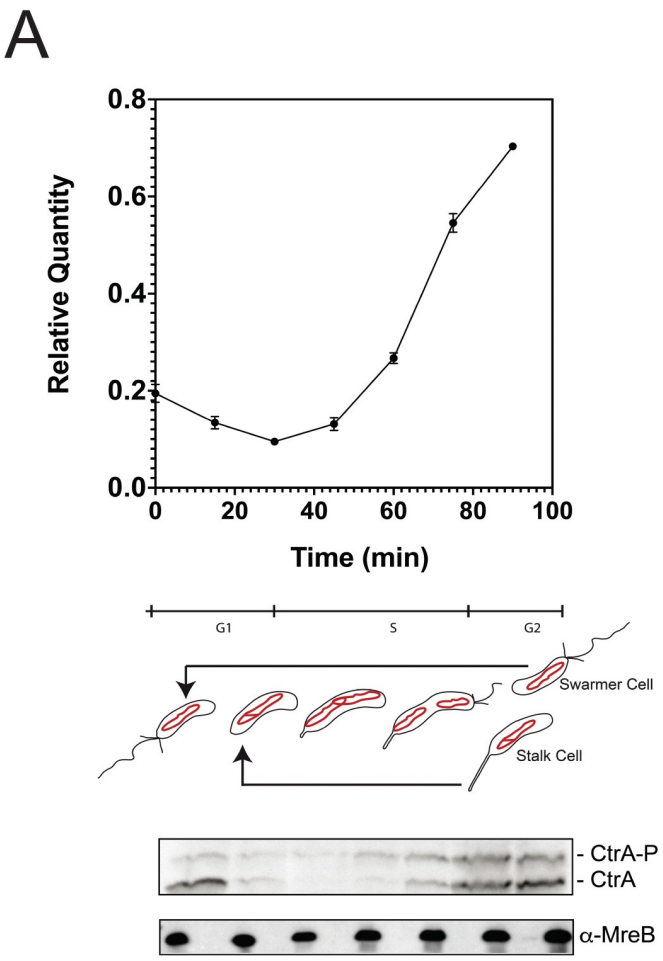

Fig 1. CcnA is a cell cycle–regulated ncRNA. (A) Expression level of CcnA during the cell cycle of WT cells *C. crescentus*. Cells were grown in PYE until OD_{600nm} = 0.6 then synchronized according to material and methods. Total RNA was extracted at indicated time points of the cell cycle. Expression of CcnA was then determined by qRT-PCR in comparison to 16S rRNA level. Results are shown as mean (N = 3) +/− SD. Data are in S9 Table. Proteins corresponding to the same time points were extracted and separated on a SDS-PAGE gel containing Phostag and Mn^{2+} to visualize CtrA phosphorylation. CtrA (Phostag) and MreB (in a normal Western blot) were revealed using specific

polyclonal antibodies on nitrocellulose membranes. (**B) Determination of the transcriptional +1 site of CcnA ncRNA by primer extension**. Total RNA extracted from WT cells or containing P*lac-ccnA* was used with a radiolabelled oligo (bold sequence in **C**). The same oligo was used for *ccnA* sequencing (CGTA). The sequence is presented as the reverse complement. The +1 signal is represented by the arrow. See S2A Fig for controls. Data are representative of 2 independent experiments. (**C) DNA 5′ sequence of *ccnA*.** Boxed gray "**G**" corresponds to the transcriptional +1. Oligo use for the sequencing and primer extension is in bold. CtrA box promoter region is underlined. CcnA, cell cycle noncoding RNA A; ncRNA, noncoding RNA; qRT-PCR, quantitative real-time PCR; WT, wild-type.

https://doi.org/10.1371/journal.pbio.3001528.g001

ncRNA involved in adaptation to carbon starvation [26]. Another ncRNA, GsrN, is involved in the response to multiple σ^T-dependent stresses [27]. Finally, ChvR has been recently characterized as a ncRNA that is expressed in response to DNA damage, low pH, and growth in minimal medium [28]. However, as more recent approaches using RNA sequencing (RNAseq) and postgenomic techniques expanded the *plethora* of ncRNA candidates to more than 100 (Zhou and colleagues, 2015). Predictions of their integration into the cell cycle circuit [29] suggest that those new candidate ncRNAs should be deeply studied in order to find whether ncRNAs are linked to cell cycle regulation. Indeed, ncRNA-mediated regulations can provide network properties that are not always easily accessible through transcriptional regulation only. For example, the phenomena like threshold-linear response of the mRNA target, the prioritization of different targets, ultrasensitive response, and bistability are known regulatory mechanisms mediated by ncRNAs [30,31], therefore representing good candidates as regulators of a biological system showing rich dynamic behavior as the *C. crescentus* cell cycle.

Here, we investigated the role of a ncRNA, named CcnA, which is transcribed from a gene located at the origin of replication of the *C. crescentus* chromosome. We characterized its role in cell cycle regulation by using deletion mutants, CcnA overexpression strains, and silenced strains obtained through expression of a CcnA antisense RNA. Results presented here identified the mRNAs of *ctrA* and *gcrA*, 2 master regulators of cell cycle, as important targets of the CcnA ncRNA. Our results are supported by a multipronged approach, combining "MS2-affinity purification coupled with RNA sequencing" (MAPS) assays, *in vitro* and *in vivo* experiments. Finally, the role of CcnA in the closely related organism *Sinorhizobium meliloti* suggests an evolutionary conservation across alphaproteobacteria, further underscoring the importance of this gene.

Results

CcnA expression is activated in predivisional cells

Based on previous results [32], we speculated that CCNA_R0094, here named cell cycle noncoding RNA A (CcnA), has its peak of transcription after the accumulation of CtrA, in the second half of the S-phase, when, the second *ctrA* promoter, P2, is activated. A synchronized population of wild-type (WT) *C. crescentus* was used to collect cells at 15-min intervals in rich medium (generation time is 96 min). We designed primers (amplifying between the 80 and 168 nt of the 182 nt long CcnA sequence; primers sequence is in S3 Table) to detect and precisely quantify CcnA RNA in the cells during cell cycle by quantitative real-time PCR (qRT-PCR) (see Materials and methods) with respect to 16S RNA levels (Fig 1A). CcnA levels start increasing after 45 min, coincidentally with CtrA protein levels (Fig 1A). More specifically, we measured both protein and phosphorylation levels of CtrA by Phos-Tag gels (Fig 1A). CcnA levels increase as CtrA~P levels increase, suggesting that the transcription of *ccnA* potentially depends on phosphorylated CtrA. This observation prompted us to question whether CtrA was involved in *ccnA* transcription. Consistent with this, a CtrA box was previously described upstream of the transcriptional start site (TSS) of *ccnA* [32,33].

We performed RNAseq using a *ctrA* thermo-sensitive allele *ctrA401ts* (*ctrA*-ts) to test for variations of *ccnA* expression in the context of the global transcriptional changes taking place in this highly perturbed mutant [11,18,34]. At the permissive temperature (30˚C), *ctrA*-ts shows a partial loss of function phenotype while the strain does not grow at the restrictive temperature (37˚C) [34]. The analysis on *ccnA* revealed that expression of CcnA is reduced in the *ctrA*-ts compared to WT at the restrictive temperature (S1A Fig), suggesting that of completely functional CtrA is required to express *ccnA*. This observation is consistent with the cell cycle–regulated profile of CcnA and with a predicted CtrA binding site in the *ccnA* promoter region. This result was further supported (S1B Fig) by the observation that CcnA shows increased levels in strains where CtrA has higher levels of stability, such as *rcdA*, *popA*, and *cpdR* mutants in which CtrA protein steady state levels are higher than the WT (S1C Fig). The increase of *ccnA* transcription in *rcdA*, *popA*, *cpdR*, and *divJ* deletion strains indeed support the hypothesis that *ccnA* transcription may be regulated by CtrA.

In summary, CcnA is a ncRNA-regulated by cell cycle and putatively regulated in a positive way by CtrA, with peak expression in the second half of DNA replication, coincident with CtrA accumulation. Considering the high affinity of CtrA on the promoter of CcnA [35], future studies are necessary in order to investigate this putative CcnA transcriptional activation by CtrA.

CcnA transcription is required for the accumulation of CtrA

To understand the function of CcnA by overexpression, we fused the sequence of *ccnA* with the first transcribed nucleotide of a P*lac* promoter in the vector pSRK [36] (see Materials and methods). This vector was introduced in *C. crescentus* cells, and its +1 nucleotide was analyzed in the overexpression strain in comparison with the WT native CcnA by primer extension (Fig 1B and 1C) (see Materials and methods). The level of CcnA in this inducible system, estimated by primer extension (Figs 1B and S2A) and quantified by qRT-PCR (S1B Fig), confirmed higher levels of CcnA expression compared to the WT. Cells overexpressing *ccnA* showed cell cycle defects, such as slow growth (Fig 2A–2C), morphologies related to abnormal cell division (Fig 2D), with an increased number of long stalks (S3 Fig). Several tests were performed in order to characterize these phenotypes and provide a basis to better understand the mechanisms behind them. By quantifying cell size parameters by using MicrobeJ [37], we discovered that cells expressing *ccnA* ectopically were significantly more elongated and filamentous than WT cells (Fig 2E). Stalk biogenesis, cell division, and inhibition of DNA replication are all under the control of CtrA [34,38], suggesting that CcnA may feedback on CtrA production to affect these processes. Indeed, upon expression/overexpression of CcnA, CtrA accumulates to higher steady state levels with respect to the control strain, while in the loading control, MreB, levels are constant (Fig 2F). We also checked the effect of high CtrA levels on the DNA replication behavior. As previously demonstrated, the overexpression of CtrA in a WT background does not induce a block of DNA replication given its cell cycle–regulated proteolysis [39]. Flow cytometry experiments showed that overexpressing CcnA indeed did not induce a change in DNA content (S4A and S4B Fig).

CtrA must be phosphorylated by a phosphorelay that includes CckA and ChpT to become fully active (S5A Fig). The Phos-tag technique, implemented as previously described [40], allowed us to evaluate the levels of CtrA~P upon overexpression of CcnA. The analysis revealed that the band of CtrA~P was more intense than the band of nonphosphorylated CtrA when CcnA was overexpressed (S5B Fig). As phosphorylation of CtrA is under the control of the phosphorelay CckA-ChpT [18], we tested whether ChpT behavior may be affected in mutants of CcnA. We used a YFP translational fusion of ChpT (ChpT-YFP) in order to understand whether CcnA ectopic expression was causing a change in protein subcellular

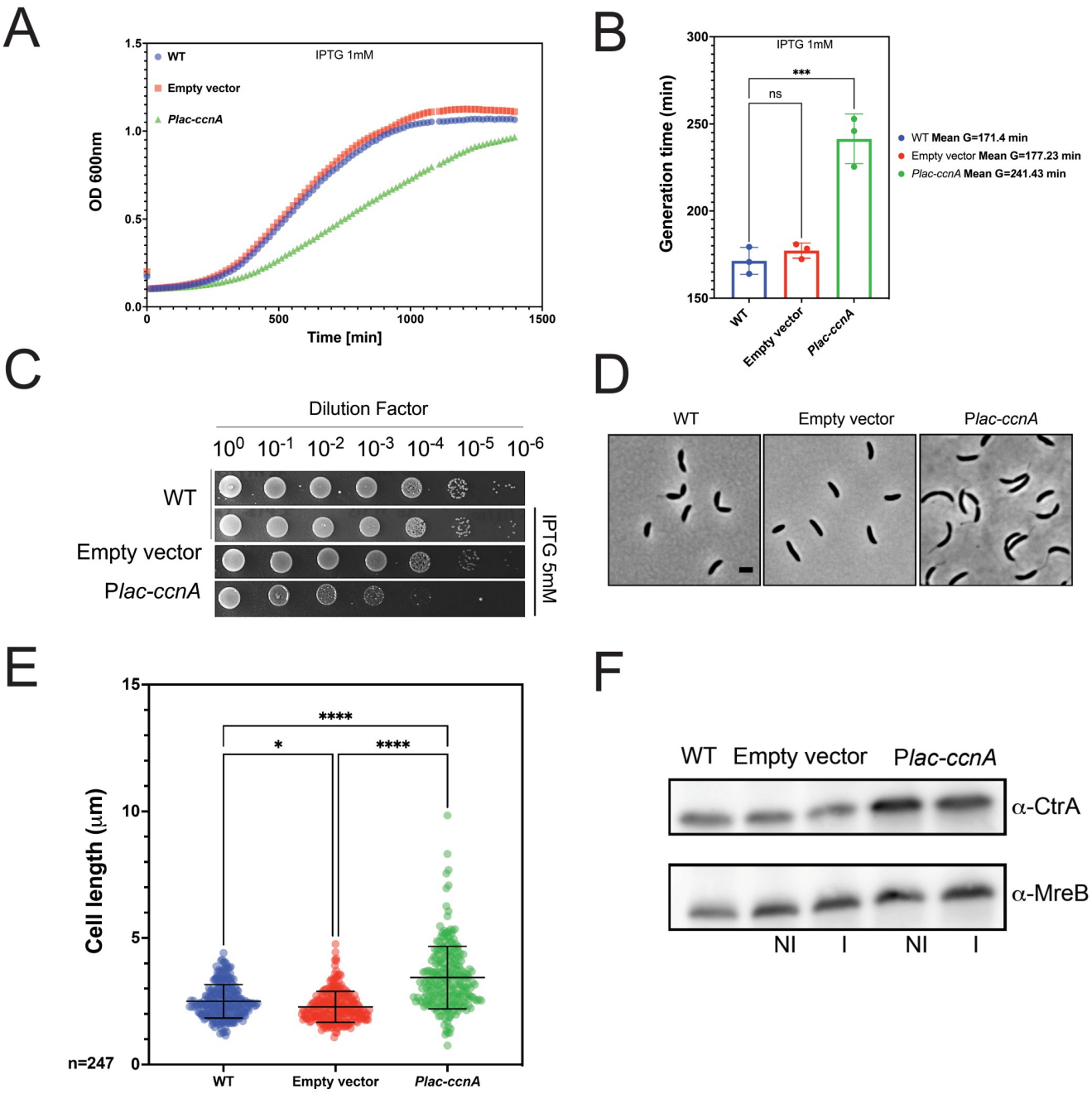

Fig 2. CcnA affects the cell cycle. (A) Growth curves following the expression of CcnA. WT cells and WT cells carrying either an empty pSRK (empty vector) or a pSRK with *ccnA* under the control of an inducible P*lac* promoter (P*lac-ccnA*) were grown in PYE without IPTG. A volume of 200 μL of cells back-diluted from stationary phase cultures to an OD_{600nm} = 0.02 were then grown on 96 wells in PYE supplemented with 1 mM IPTG. Cell growth was monitored overnight with a Spark-TM at 30˚C and a shaking (orbital) amplitude of 6 mm and a shaking (orbital) frequency of 96 rpm. Results are shown as mean $N = 3$ biological replicates with 3 technical replicates. Raw data are provided in S7 Table. **(B) Determination of the doubling time of cells expressing CcnA**. Doubling times of cells from (2A) were calculated by using the exponential growth equation (nonlinear regression) (Prism GraphPad 9.1.2). Statistical analysis was performed using ANOVA with a Brown–Forsythe and Welch ANOVA tests and a Dunnett's multiple comparisons test. ns, difference not significant, ***: p.val = 0,0002. Data are in S9 Table. **(C)** WT cells, WT cells carrying either an empty vector or P*lac-ccnA* were grown overnight in PYE at 30˚C and diluted to an OD_{600nm} = 0.6. Samples were then serially diluted (10^0–10^{-6}) and 4.5 μL of each dilution were spotted on a PYE-Agar + 5 mM IPTG plate and incubated at 30˚C. WT cells without plasmid were used as negative control. **(D)** Phase contrast images of WT cells, WT cells carrying an empty vector or P*lac-ccnA* grown in PYE without IPTG until OD_{600nm} = 0.6. Scale bar = 2 μm. **(E)** Cells from (2D) were analyzed using MicrobeJ [37] to assess cell length. Approximately 247 cells were analyzed for each condition, and statistical significance was determined using ANOVA with Tukey multiple comparisons test. *: p.val = 0.0168 ****: p.val < 0.0001. Raw Data are provided in S8 Table. **(F)** WT cells, WT cells carrying an empty vector or *Plac-ccnA* were grown in PYE at 30˚C until OD_{600nm} = 0.6. Then, induction of P*lac-ccnA* was made by addition of IPTG 1 mM 30 min. As a

control of induction, WT cells carrying an empty vector were also incubated 30 min in presence of IPTG 1 mM and WT cells with no induction were used as a control (NI = no IPTG) and (I = IPTG). Proteins were extracted and separated on a SDS-PAGE gel for Western blotting. CtrA and MreB (loading control) proteins were revealed using specific polyclonal antibodies on nitrocellulose membranes. Results are representative of at least 2 independent experiments (see S14 Fig for additional westerns). In comparison with the control strain (empty vector), cells over expressing CcnA show + 78% and + 54% of CtrA in NI and I conditions, respectively. CcnA, cell cycle noncoding RNA A; WT, wild-type.

https://doi.org/10.1371/journal.pbio.3001528.g002

localization and levels. Epifluorescent microscopy was used to observe the protein level of ChpT-YFP (S5C Fig). Data were further analyzed by MicrobeJ (Materials and methods), and results were compared to a strain carrying an empty vector showing that upon CcnA overexpression intensity and clustering of the signal increase in the ChpT-YFP strain background, more specifically in elongated cells with long stalks (S5D and S5E Fig). Finally, we tested by Western blot whether CcnA overexpression affected the protein level of ChpT, using antibodies against the GFP protein that does recognize YFP and compared the levels of the ChpT-YFP translational fusion in strains carrying either an empty vector or CcnA. Our results showed that upon overexpression of CcnA, YFP-ChpT levels were higher than those of the empty vector (S5F Fig). This observation may suggest that CcnA overexpression increases CtrA phosphorylation by affecting the localization and levels of ChpT by an unknown mechanism so far.

In conclusion, an increase in CcnA expression induces an increase in the steady state levels of CtrA protein, specifically in its phosphorylated form (CtrA~P). These changes in the CtrA levels may well explain the cell cycle defects observed at the morphological and molecular levels, notably increase of cell length, and long stalks.

The gene *ccnA* is located in the origin of replication (Fig 3A); therefore, its sequence, at least partially, plays an essential role in the initiation of replication [41,42]. We attempted a complete deletion of the *ccnA* sequence by 2-step recombination in the presence of an extra copy of *ccnA* (Materials and methods), as previously described [43]. Considering that *ccnA* coincides with an essential part of the origin of replication of the genome, the deletion of the *ccnA* sequence was not successful, demonstrating that the genomic sequence of *ccnA* is essential [41]. We then applied different strategies to inactivate partial sequences of *ccnA* that kept most of the origin of replication intact (S6 Fig) without success. Finally, we attempted to delete the 45-bp long promoter region containing the CtrA box. The *ccnA* expression should be under the control of CtrA; therefore, we hypothesized that the deletion of its box in the promoter region should have a mild or no effect on the origin but impair the expression of the ncRNA. The deletion of the promoter region was obtained, and the expression of *ccnA* in the corresponding mutant was first tested by primer extension (Figs 3B and S7A) that showed the absence of CcnA. We also used qRT-PCR (S1B Fig) using primers for *ccnA* and the 16S sequence as reference (Materials and methods) in order to quantify the decrease of CcnA upon deletion of its putative promoter (Δ*prom* mutant). Upon deletion of the promoter region, we observed a significant decrease of CcnA expression that may explain the cell cycle defects (phenotypes that are similar to silencing approach; see below) (S1B Fig).

The Δ*prom* mutant was analyzed by growth curves (Fig 3C), and its morphology was observed by microscopy (S8A Fig). This strain showed slow growth and more precisely a longer lag phase than the WT strain (Fig 3C). Western blots were performed using antibodies against CtrA and MreB (Fig 3D). This mutant showed a decrease of CtrA steady state levels, as expected considering the opposite effects in the overexpression strain (Fig 2F). On the contrary, MreB (loading control) remained stable, suggesting a specific effect on CtrA. As the deletion of *ccnA* promoter removes also some elements of the origin of replication [42], we performed flow cytometry analysis on synchronized populations to understand whether the deletion of *ccnA* promoter of *C. crescentus* does not interfere with DNA replication initiation. Flow cytometry analysis revealed that the markerless deletion of *ccnA* promoter does not have a

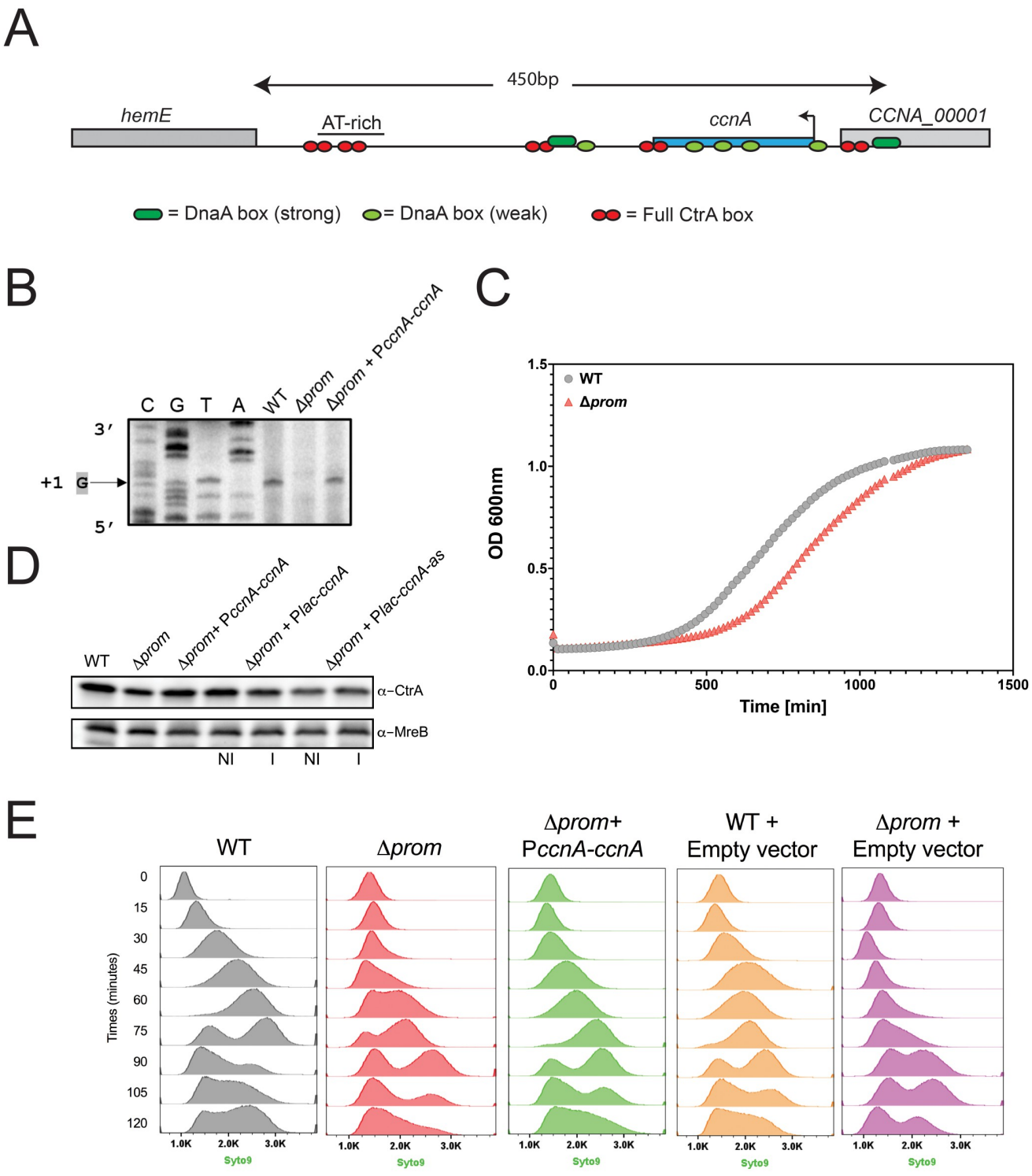

Fig 3. Δ*prom* cell cycle defects are rescued by CcnA *in trans* under the control of its own promoter. (A) Schematic representation of the origin of replication and *ccnA* gene locus in *C. crescentus*. The origin of replication contains 5 full CtrA boxes, 2 strong and 5 weak DnaA boxes [44]. Transcription of *hemE* gene is important for DNA replication and can be negatively regulated by CtrA when present [44,45]. The chromosome replication initiator protein DnaA unwinds the DNA from the AT Rich region on the chromosome when CtrA is absent. The *ccnA* gene is 182 nt long and contains 3 DnaA weak boxes, a CtrA box in its promoter region and a CtrA box in its terminal region. **(B) Determination of the transcriptional +1 site of CcnA ncRNA by primer extension**. Total RNA extracted from WT cells, deleted *ccnA* promoter (*Δprom*), and containing P*ccnA-ccnA* (*Δprom* + P*ccnA-ccnA*) were used with radiolabelled oligo. The same oligo was used for *ccnA* sequencing (CGTA). The +1 signal is represented by the arrow. See S7A Fig for

controls. Data are representative of 2 independent experiments. **(C) Growth curves of cells deleted from *ccnA* promoter.** WT cells and Δ*prom* cells were grown overnight in PYE at 30˚C. A volume of 200 μL of cells back-diluted from stationary phase cultures to an OD_{600nm} = 0.02 were then grown on 96 wells in PYE. Cell growth was monitored overnight with a Spark-TM at 30˚C and a shaking (orbital) amplitude of 6 mm and a shaking (orbital) frequency of 96 rpm. Results are shown as mean *N* = 2 biological replicates with 3 technical replicates. Raw data are provided in S7 Table. **(D)** WT cells, Δ*prom* cells, Δ*prom* cells carrying either a pMR10 low-copy plasmid harboring *ccnA* under the control of its own promoter (Δ*prom* + P*ccnA-ccnA)* or *ccnA* or its antisense under the control of a P*lac* promoter (Δ*prom*+ P*lac-ccnA*, Δ*prom* + P*lac-ccnA-as)* were grown in PYE at 30˚C until OD_{600nm} = 0.6. For Δ*prom*+ P*lac-ccnA*, Δ*prom* + P*lac-ccnA-as* cells, expression of *ccnA* or its antisense was made by addition of IPTG 1 mM 30 min. Proteins were extracted and separated on a SDS-PAGE gel for western blotting. CtrA and MreB (loading control) proteins were revealed using specific polyclonal antibodies on nitrocellulose membranes. Results are representative of at least 2 independent experiments with similar results (see S7B and S14D Figs for controls). **(E)** Flow cytometry profiles after SYTO 9 staining showing DNA content of synchronized WT cells, Δ*prom* cells, Δ*prom* cells carrying *ccnA* under its own promoter (Δ*prom* + P*ccnA-ccnA)* and as controls WT cells carrying an empty low-copy plasmid pMR10 (WT + empty vector) or *Δprom* cells carrying and empty low-copy plasmid pMR10 (Δ*prom* + empty vector). Synchronization of cells was performed as described in Material and methods. Pure G1 (1N) swarmer cells were isolated by Percoll for density gradient, and DNA replication over the cell cycle was followed on synchronized cells at different time point. A total number of 300,000 particles were analyzed by flow cytometry using the blue laser (488 nm) and filter 525/30 nm. Results are representative of 3 biological replicates. CcnA, cell cycle noncoding RNA A; ncRNA, noncoding RNA; WT, wild-type.

https://doi.org/10.1371/journal.pbio.3001528.g003

strong effect on DNA replication but probably causes a delay in the initiation of DNA replication (Fig 3E). Given the lower level of CtrA in the *Δprom* strain, we would expect DNA replication to occur at a higher rate in this mutant. However, we observed normal initiation of DNA replication in the WT strain with a shift in peak intensity from 30 min of the cell cycle demonstrating that DNA replication has begun and a total shift from 1 chromosome (1N) to 2 chromosomes (2N) at 60 min whereas the *Δprom* strain remained blocked with 1N until 60 min and began to accumulate 2N content only at 60 min given the second peak that was observed. We estimated the percentage of 1N in *Δprom* cells at 34.65% +/− 3.88% and 2N at 63.85% +/- 3.46%.

We complemented the *Δprom* strain with a WT copy of *ccnA* under the control of its own promoter in a low-copy vector (*PccnA-ccnA*). We were interested in understanding whether a deletion of a portion of *CORI* was the sole reason of the *Δprom* phenotypes or whether it was due to a lack of *ccnA* transcription.

Indeed, the Δ*prom* was almost entirely complemented by an extra copy of the *ccnA* gene, as DNA replication (Fig 3E), growth (S8B Fig), and CtrA levels (Fig 3D) were rescued by the extra copy of CcnA, demonstrating that the phenotype of Δ*prom* was mostly related to the absence of CcnA.

An alternative, less invasive strategy with respect to the origin of replication was to overexpress an antisense of CcnA (CcnA-as) in order to silence the RNA of CcnA. A reverse complementary sequence of *ccnA* driven by a P*lac* promoter was cloned, as described in the previous section for the sense sequence and expressed in *C. crescentus* in order to demonstrate a negative effect on CcnA activity. Based on western blots, the expression of the CcnA-as, as the Δ*prom* strain, showed a decrease of CtrA steady state levels (S9A Fig). Flow cytometry analysis also showed an accumulation of chromosomes ($N \geq 3$) in the presence of CcnA-as (S9B and S9C Fig). Moreover, an increase of doubling time was observed (S9D Fig). These results suggested that the expression of the antisense phenocopy Δ*prom*, so it may indicate an inactivation of CcnA activity. This result, together with the viability of the *ccnA* Δ*prom* strain, also suggests that the inactivation of CcnA is not lethal.

In conclusion, both overexpression and low levels of CcnA showed consistent results that suggested that CcnA promotes the accumulation of CtrA and possibly other genes expression products. Therefore, we wondered if this activity was due to a direct binding by CcnA to the 5′ untranslated region (5′ UTR) of *ctrA* and potentially other genes.

CcnA potentially interacts with mRNAs of *ctrA*, *gcrA*, and other cell cycle genes

In order to identify RNAs that were targeted in vivo by CcnA and test whether *ctrA* mRNA was a direct target of CcnA, we performed the technique called MAPS (MS2-affinity

purification coupled with RNA sequencing) as previously described [46]. This technique relies on the fusion of a ncRNA of interest with the RNA aptamer MS2 used as a tag at the 5′ of the ncRNA. MAPS approach involves the use of a protein called MS2-coat with a high affinity for the MS2 RNA aptamer. This technique allows the identification of RNAs or proteins directly interacting with a tagged RNA (S10 Fig). We indeed constructed a version of CcnA tagged with an MS2 RNA aptamer able to bind the protein MS2-MBP immobilized on an amylose resin. As a negative control, an untagged *ccnA* was cloned in order to compare results specific to the MAPS technique. Strains expressing MS2-*ccnA* or *ccnA* (introduced in the same pSRK plasmid type previously used for *ccnA* overexpression) were lysed, and soluble cell content was loaded onto an amylose column containing MS2-MBP fusion. RNA was purified as previously described (Materials and methods) [46].

Eluted RNAs, trapped in the amylose column in the presence of MS2-CcnA or non-tagged CcnA, were characterized by RNAseq, and results were analyzed (S1 Table; see Materials and methods for a detailed protocol of analysis). First, as a control, we looked for the presence of reads in the vicinity of *ccnA* only in the MS2-CcnA strains (S11A Fig). Among other candidate targets (S12 Fig), the *ctrA* mRNA was detected (S11B Fig). This result is in accord with our previous results that CcnA overexpression and down-regulation affected CtrA expression. The extent of CcnA-regulated targets is bigger than just *ctrA* mRNA. As shown in S12 Fig and S1 Table, other mRNAs, including *gcrA*, are potentially targeted by CcnA. A general observation of candidate targets of CcnA is that most of them belong to the CtrA and GcrA regulons, such as those encoding motility proteins (S12 Fig, S1 Table).

We also tagged the 5′ UTRs of *ctrA* with the MS2 aptamer (mRNAs generated by its P1 or P2 promoter) in order to determine the putative interaction with CcnA. We expressed the MS2-tagged UTRs in *C. crescentus* cells, and we looked for the enrichment of CcnA in the MS2-P1 and MS2-P2 UTRs associated to the correct overexpression of the 5′ UTRs (S11C Fig). We demonstrated that only the UTR of *ctrA* mRNA transcribed by the P2 promoter pulls down CcnA (S11D Fig). Although P1 obviously contains the sequence present in P2, it may form different secondary structures that could mask the CcnA binding regions. This final result consolidates the observation that CcnA may be indeed associated *in vivo* with the 5′ UTR of *ctrA* expressed by the promoter P2 and not by P1. We also analyzed all possible interaction candidates bound to the 5′ UTR of *ctrA* P1 and P2 (S1 Table). This analysis revealed that several other noncharacterized ncRNAs might interact with the P1 and P2 5′ UTRs of *ctrA*. Their specific role should be investigated in future studies.

CcnA binds *ctrA* and *gcrA* mRNAs *in vitro*

MAPS revealed a putative interaction between CcnA and P2-5′ UTR of *ctrA* and, interestingly, among master regulators of cell cycle, the *gcrA* mRNA (S1 Table, S12 Fig). To better characterize/validate these interactions, we performed *in vitro* probing experiments. Results showed 2 regions of protection by CcnA for *ctrA* 5′ UTR from the promoter P2 (Fig 4A). Concerning the *gcrA* mRNA 5′ UTR, we used data derived from 5′ RACE experiments at the genome scale [32]. Results obtained with *in vitro* probing experiments for *gcrA* 5′ UTR instead showed only one region of protection by CcnA (Fig 4B). A common feature of both *gcrA* and *ctrA* P2 protections by CcnA was the sequence 5′-GGGG-3′ (Fig 4A and 4B) that corresponds to the region of CcnA belonging to a loop (Loop A) (Fig 4C). EMSA experiments using P2-*ctrA* and *gcrA* 5′ UTRs confirmed the interaction with CcnA (WT). The binding is diminished with a CcnA mutated in the Loop A ($CcnA_{GGGG}$) (Fig 5A–5F). We also performed EMSA on mutated P2-*ctrA* (P2-$ctrA_{CCCC}$) and *gcrA* ($gcrA_{CCCC}$), and there was also a decrease of the CcnA binding (S2B and S2C Fig). However, $CcnA_{GGGG}$ was not able to compensate the mutations on P2-

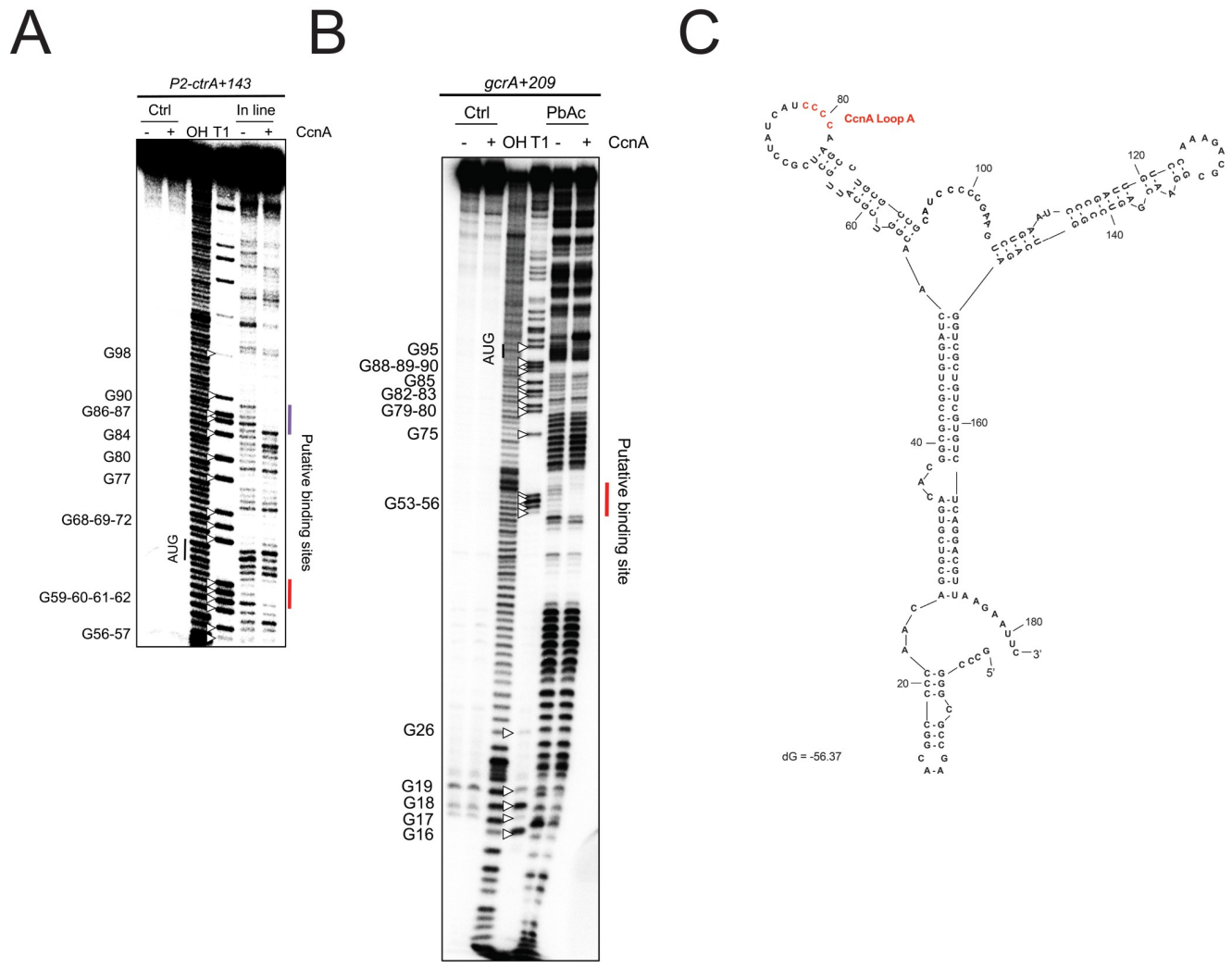

Fig 4. CcnA interacts directly *in vitro* with the 5′ UTR of P2-*ctrA* mRNA and 5′ UTR of *gcrA* mRNA. (A) Inline ($MgCl_2$) probing of 5′ end-radiolabeled P2-*ctrA*+143 incubated in presence (+) or absence (−) of CcnA ncRNA. OH, alkaline ladder; T1, RNase T1 ladder. The numbers to the left indicate sequence positions with respect to the +1 of the transcript. **(B)** Lead acetate probing of 5′ end-radiolabeled *gcrA*+209 incubated in presence (+) or absence (−) of CcnA ncRNA. OH, alkaline ladder; T1, RNase T1 ladder. The numbers to the left indicate sequence positions with respect to the +1 of the transcript. **(C)** Secondary structure of CcnA RNA predicted using mFold algorithm [48]. The predicted free energy of the thermodynamic ensemble is −56.37 kcal/mol. CcnA Loop A is shown in red and is composed of a stretch of « CCCC ». CcnA, cell cycle noncoding RNA A; ncRNA, noncoding RNA; 5′ UTR, 5′ untranslated region.

https://doi.org/10.1371/journal.pbio.3001528.g004

ctrA or *grcA* 5′ UTRs. Considering the putative importance of the Loop A for the interaction between CcnA, *ctrA*, and *gcrA* mRNAs, we searched for the presence of the GGGG motif in the 5′ UTRs of MAPS targets (S1 Table) in comparison with a dataset of UTRs randomly selected in the genome of *C. crescentus*. Results showed that 35% of CcnA-bound MAPS-positive candidate targets possessed GGGG (p-value = 0.02) (S12 Fig).

As a stretch of CCCC, present in the Loop A region of CcnA, is protecting a putatively conserved GGGG motif in P2 *ctrA* 5′ UTR and *gcrA* 5′ UTR, we constructed mutant of CcnA of the Loop A by introducing mutations in the active loop "CCCC to GGGG" ($CcnA_{GGGG}$). This mutated version of CcnA was then tested *in vivo* using the same pSRK expression system as previously. The mutation $CcnA_{GGGG}$ in Loop A reduced the growth defect phenotype of CcnA overexpression (Fig 6A–6C). Flow cytometry analysis of the Loop A mutant revealed a

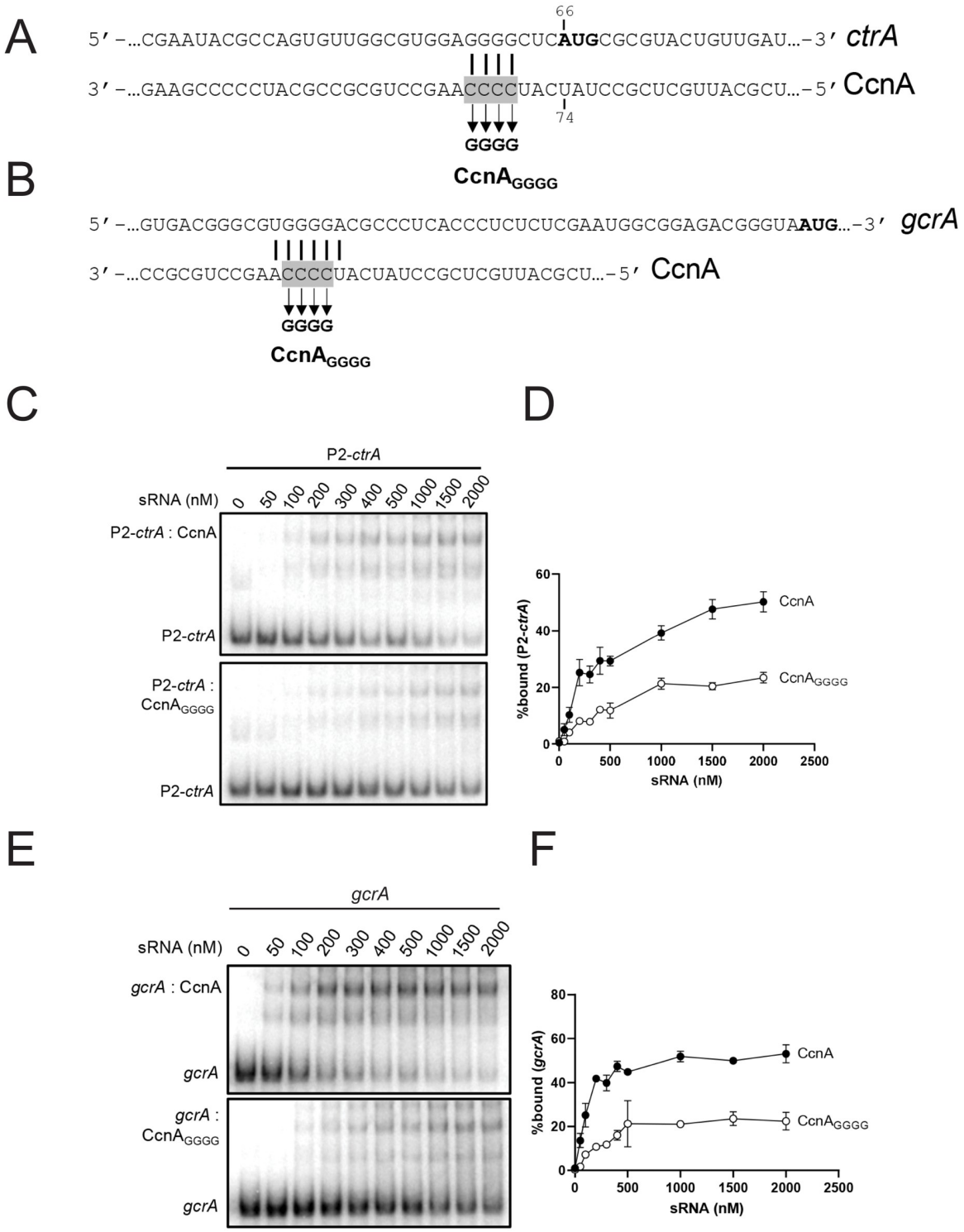

Fig 5. CcnA mutation of Loop A decreases the interaction with the 5′ UTR of P2-*ctrA* mRNA and 5′ UTR of *gcrA* mRNA. (A) Mutation of the *ctrA* mRNA (*ctrA*$_{GGGG}$) and ncRNA CcnA (CcnA$_{GGGG}$) binding site (shown in red in Fig 4A). Solid lines indicate CcnA binding sites on *ctrA*. Boxed gray text corresponds to the nucleotides mutated. The translation start codon is shown in bold. **(B)** Mutation of the *gcrA* mRNA (*gcrA*$_{GGGG}$) and ncRNA CcnA (CcnA$_{GGGG}$) binding site (shown in red in Fig 4B). Solid lines indicate CcnA binding sites on *gcrA*. Boxed gray text corresponds to the nucleotides mutated. **(C)** A final concentration of 5 nM of P2-*ctrA* (+143 nt from the P2-*ctrA* promoter) RNA fragment was incubated with increasing concentration of CcnA (top) or CcnA$_{GGGG}$ (bottom) ncRNA. % bound RNA with ncRNA CcnA (black) or CcnA$_{GGGG}$ (white) is showed (**D**). Data represent the mean of 2 independent

experiments ± SD. Data are in S9 Table. (**E**) A final concentration of 5 nM of *gcrA* RNA fragment was incubated with increasing concentration of CcnA (top) or $CcnA_{GGGG}$ (bottom). % bound RNA with ncRNA CcnA (black) or $CcnA_{GGGG}$ (white) is showed (**F**). Data represent the mean of 2 independent experiments ± SD. Data are in S9 Table. CcnA, cell cycle noncoding RNA A; ncRNA, noncoding RNA; 5′ UTR, 5′ untranslated region.

https://doi.org/10.1371/journal.pbio.3001528.g005

dominant negative phenotype similar to the antisense expression with accumulation of chromosomes ($n \geq 3$) (Fig 6D and 6E). These results suggest that the growth defect phenotype observed when inducing the WT version of CcnA could be mainly due to the interaction of the Loop A of CcnA to the mRNAs of *gcrA* and *ctrA*. As the interaction between CcnA and GcrA was confirmed *in vitro*, we asked whether this binding was suggesting a possible regulation of CcnA on the GcrA protein levels. Therefore, we used the overexpression of CcnA and measured the level of GcrA using western blot and anti-GcrA antibodies. The analysis of GcrA in a *ccnA* overexpression strain revealed a decrease of GcrA steady state protein levels in comparison with a WT strain carrying the empty vector (S14B Fig), suggesting the presence of both a CtrA-mediated inhibition of *gcrA* transcription and, in addition, a direct effect on GcrA expression by CcnA binding to its mRNA. However, besides showing a direct interaction between CcnA and the 5′ UTR of *gcrA*, we are not able to disentangle the effect of CtrA regulation on GcrA activity from a potential direct regulation of the *gcrA* mRNA by CcnA.

Taken together, those results suggest that the region corresponding to Loop A plays a significant role in the CcnA activity, confirming both the *in vitro* and the MAPS results shown previously. However, other regions can definitely play important roles in the activity of CcnA that will require further analysis. Moreover, CcnA seems to have a second important target in the cell, GcrA, for which the ncRNA potentially plays a negative role. Further analysis using INTA RNA [47] confirmed that at the prediction level those UTRs are potentially able to interact with the LoopA region of CcnA (S14E Fig).

CcnA affects the CtrA and GcrA regulons

RNAseq was used to compare the strains overexpressing *ccnA* to the strains expressing *ccnA-as* in biological triplicates in order to reveal RNAs affected by CcnA with the hypothesis that it may show links with CtrA and GcrA regulons.

Differentially expressed genes (DEGs), identified when comparing the sense and antisense expressing strains, were considered for the analysis (S12 Fig, S2 Table). These results were also integrated with additional information such as (i) the presence of full or half CtrA binding boxes as identified by a Position Weight Matrix scan of the *C. crescentus* genome [33]; (ii) the abundance of reads from a ChIP-Seq experiment aimed at characterizing GcrA occupancy [15]; (iii) the genes whose expression levels change significantly in a Δ*ccrM* strain [49]; (iv) the essential genes as revealed with Tn-seq [41]; (v) genes with cell cycle–dependent expression [50]; (vi) genes positive in MAPS; and, finally, (vii) genes possessing the motif GGGG (complementary to CcnA LoopA). The analysis revealed 215 genes differentially expressed between the 2 conditions (CcnA versus CcnA-as). The CtrA regulon is composed of genes activated and repressed by the phosphorylated form of CtrA, which recognizes a full palindromic or half site [32]. Among the 215 genes, we found a statistically significant enrichment of CtrA binding sites, both half and full [33]. To calculate significance of enrichments, we used a one-sided binomial exact test (binom.test in R) and got a p-value = 0.0065 for the full site, and a p-value = 0.0001 for the half site. This finding suggests that upon changes of CcnA levels, the most affected regulon is CtrA's.

We also looked for DEGs that could be part of the GcrA regulon. Many genes identified contained a GcrA binding region, suggesting that the GcrA regulon is differentially modulated

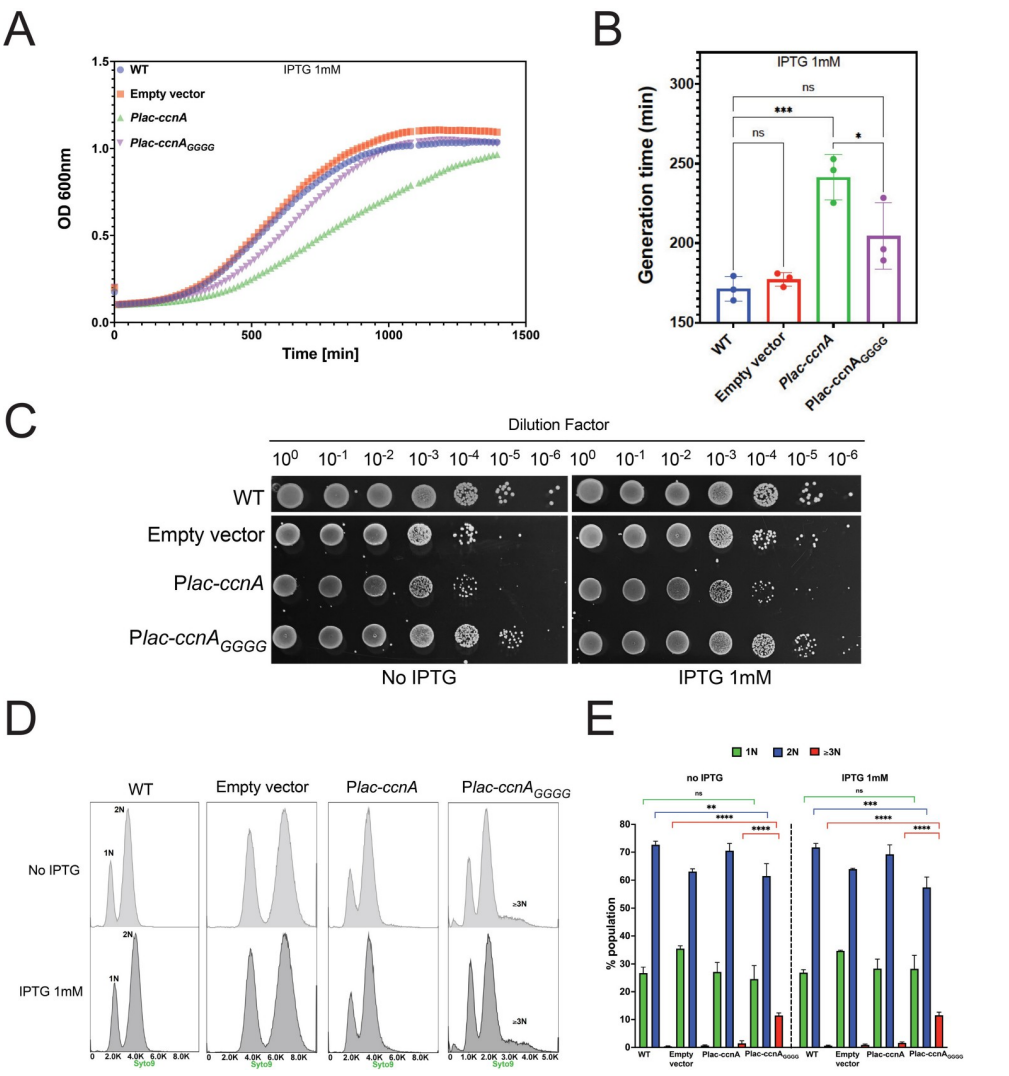

Fig 6. CcnA Loop A mutant shows attenuated cell cycle defects. (A) Growth curves following the expression of CcnA mutated in its Loop A (*Plac-ccnA$_{GGGG}$*). WT cells and WT cells carrying either an empty pSRK (empty vector) or a pSRK with *ccnA* under the control of an inducible P*lac* promoter *(Plac-ccnA)* or *Plac-ccnA$_{GGGG}$* mutated in its loop A were grown overnight in PYE without IPTG. A volume of 200 μL of cells back-diluted from stationary phase cultures to an OD_{600nm} = 0.02 were grown on 96 wells in PYE supplemented with 1 mM IPTG. Cell growth was monitored overnight with a Spark-TM at 30˚C and a shaking (orbital) amplitude of 6 mm and a shaking (orbital) frequency of 96 rpm. Results are shown as mean $N = 3$ biological with 3 technical replicates. Raw data are provided in S7 Table. Note that all growth curves data of Figs 2, 6, and S9 were acquired in the same days of their respective biological replicates and compared to each other. **(B) Determination of the doubling time of cells expressing *Plac-ccnA$_{GGGG}$*.** Doubling times of cells from (6A) were calculated by using the exponential growth equation (nonlinear regression) (Prism GraphPad 9.1.2). Statistical analysis was performed using ANOVA with a Brown–Forsythe and Welch test with a Dunnett's multiple comparisons test. ns, difference not significant, *: p.val = 0.0396 ***: p.val = 0.0009. Raw data are provided in S7 Table. **(C)** WT cells, WT cells carrying an empty vector, *Plac-ccnA* or *Plac-ccnA$_{GGGG}$* were grown overnight in PYE at 30˚C and diluted to an OD_{600nm} = 0.6. Samples were then serially diluted (10^0–10^{-6}), and 4.5 μL of each dilution were spotted on a PYE-Agar plate with or without IPTG 1 mM and incubated at 30˚C. WT cells without plasmid were used as negative control. **(D)** Flow cytometry profiles after SYTO 9 staining showing DNA content of WT cells, WT cells carrying either an empty pSRK (empty vector) *ccnA* under the control of a *Plac* promoter (P*lac-ccnA*) or *ccnA* Loop A variant (*Plac-ccnA$_{GGGG}$*) grown in PYE until OD_{600nm} = 0.3. Then, induction of P*lac-ccnA* or P*lac-ccnA$_{GGGG}$* was made by addition of IPTG 1 mM 30 min. Cells without induction were grown for an additional 30 min as a control of growth phase. A total number of 300,000 particles were analyzed by flow cytometry. **(E)** Proportions of cells harboring 1N, 2N, and ≥3N DNA in the population were analyzed by gating the histograms in (E). Data are representative of 3–5 biological replicates. Statistical analyses were carried out using ANOVA Tukey test. ns, difference not significant, **: p.val < 0.01, ***: p.val < 0.001, ****: p.val < 0.0001. CcnA, cell cycle noncoding RNA A; WT, wild-type.

https://doi.org/10.1371/journal.pbio.3001528.g006

in presence (*ccnA*) or absence (*ccnA-as*) of CcnA. Most of the genes of S12 Fig are cell cycle regulated as expected considering that both GcrA and CtrA are controlling those genes (S12 Fig). Therefore, RNAseq allowed getting a full picture of the effects of CcnA activity perturbations, which affect a significant fraction of the transcriptome involved in cell cycle regulation.

We also tested if genes affected by overexpression and inactivation of CcnA were also potentially interacting with CcnA, as revealed by MAPS analysis (S12 Fig, S1 Table). Results showed that several genes that change expression levels in mutants of CcnA are in fact putative direct targets of the ncRNA. Among those genes, many possessed the GGGG motif. For example, among the cell cycle regulators (highlighted in red in S12 Fig), we found the mRNA encoding the transcriptional regulator MraZ, involved in negative regulation of cell division processes in *E. coli* [51], the GGDEF diguanylate cyclase DgcB, the flagellar protein FlaG, or the polar organelle development protein PodJ. In addition, *rodZ* mRNA was also found among the CcnA targets and is involved in cell elongation regulation and localizes at PG synthesis sites within the cell [52]. Interstingly, a new study revealed genes expression changes following a cold stress in *C. crescentus* and identified the ncRNAs that are up-regulated under this stress. In particular, 31 ncRNAs including CcnA were conditionally expressed. In this study, CcnA was identified as the most up-regulated ncRNA (11-fold), further suggesting that CcnA may also be involved in a posttranscriptional response to cold stress [53]. These findings are consistent with the *in vivo* targets of CcnA identified in our study, which are the mRNAs of *cspA* and *cspB* encoding 2 cold shock proteins CspA and CspB [54]. Despite our primary goal to associate CcnA with the cell cycle, these data nonetheless support that CcnA might also have a significant role in responding to environmental stress. In the future, it will be worth testing the response to various stresses as cold stress or osmotic stress using mutants of *ccnA* to understand its role during unfavorable conditions.

In conclusion, the RNAseq results consolidate the potential effect of CcnA on CtrA and GcrA regulons as regulator of CtrA and GcrA protein levels but also showing a CcnA link with mRNAs of genes controlled by those master regulators as revealed by MAPS. Moreover, the overexpression of *ccnA-as* shows opposite effects than the overexpression of WT *ccnA*.

Overexpression of CcnA complements cell cycle defects

As CcrM-dependent adenosine methylation sites (GAnTC) are connected to *ctrA* transcription by its own P1 promoter, we asked whether the expression of CcnA (or its antisense) was rescuing the Δ*ccrM* mutant cell cycle severe phenotype [55], considering that CcrM methylation is required to recruit GcrA at the P1 promoter region and therefore activate *ctrA* transcription [17] (S13 Fig). We attempted to introduce the plasmid containing *ccnA* and *ccnA-as* in the *ΔccrM* mutant and analyzed the different phenotypes. First, we were unable to introduce the plasmid carrying *ccnA-as* into Δ*ccrM*, suggesting an incompatibility between the 2 genetic constructs, while the electroporation frequency for WT was as expected. This can be explained considering that both CcrM and CcnA are important to properly express CtrA; therefore, removing both mechanisms may be lethal. On the contrary, the expression of CcnA in Δ*ccrM* was viable and indeed able to suppress cell cycle defects of the mutant (Fig 7A). Notably, the severe morphological defects of Δ*ccrM* were rescued (Fig 7A–7C), as well as the motility defects (Fig 7D). We also noticed that Δ*ccrM* cells rescued by CcnA were not curved (S14A Fig). This suggests that Δ*ccrM* still retains some of the features that are independent from CtrA, as the cell curvature depends on the gene *creS* (whose expression depends on GcrA and methylation) encoding for the crescentin responsible for the cell curvature of *C. crescentus* [17].

We asked whether CcnA was indeed able to increase CtrA steady state levels in the Δ*ccrM* strain (Fig 7E). As most of the GcrA-CcrM–dependent promoters, *ctrA* P1 is sigma-70

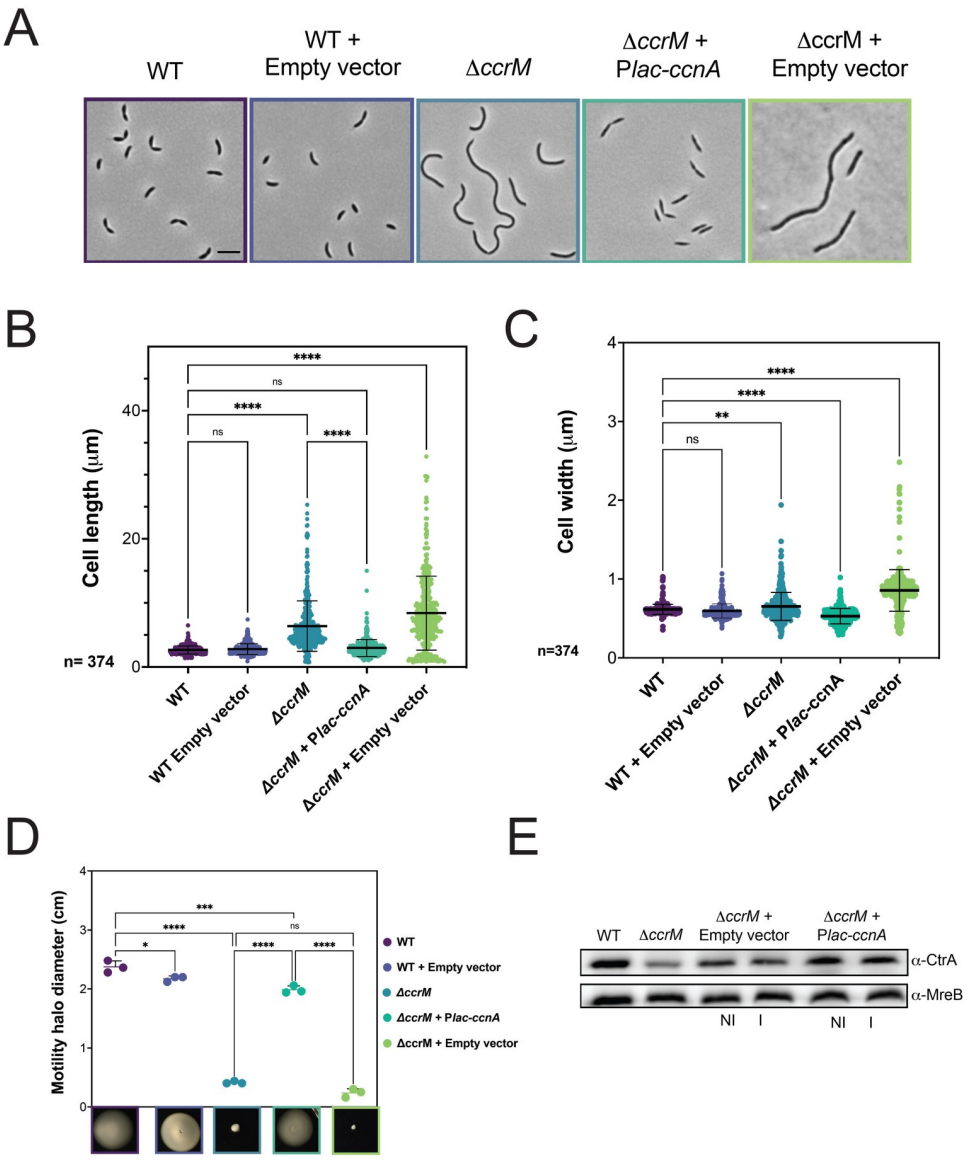

Fig 7. CcnA rescues the CcrM loss of function phenotype. (A) Phase contrast images of WT cells, WT cells carrying an empty pSRK (empty vector), Δ*ccrM* cells, Δ*ccrM* carrying a plasmid with *ccnA* under the control of a P*lac* promoter (Δ*ccrM*+ P*lac-ccnA*) or Δ*ccrM* cells carrying an empty vector (Δ*ccrM*+ empty vector) grown in PYE at 30˚C until OD_{600nm} = 0.6. Scale bar = 2 μm. **(B, C)** Cells from (7A) were analyzed using MicrobeJ [37], and 374 cells were analyzed to assess cell length and cell width. Statistical significance was determined using ANOVA with Šídák's multiple comparisons test. ns, difference not significant **: p.val = 0.0050 ****: p.val < 0.0001. Raw data are provided in S8 Table. **(D) Swarming assay on 0.25% soft agar plates.** A volume of 1 μL of each culture from cultures of Fig 7A was deposited into the soft agar and incubated at 30˚C for 5 to 6 d. *N* = 3. The diameter in cm of each mobility halo was measured with Fiji and reported in S4 Table. Statistical significance was determined using ANOVA with Šídák's multiple comparisons test. ns, difference not significant *: p.val = 0.0406, ***: p.val = 0.0003, ****: p.val < 0.0001. Data are in S9 Table. **(E)** WT cells, Δ*ccrM* cells, Δ*ccrM* cells carrying an empty vector or P*lac-ccnA* were grown in PYE at 30˚C until OD_{600nm} = 0.6. Then, induction of P*lac-ccnA* was made by addition of IPTG 1 mM 30 min. As a control of induction, *ΔccrM* cells carrying an empty vector were also incubated 30 min in the presence of IPTG 1 mM. Proteins were extracted and separated on a SDS-PAGE gel for Western blotting. CtrA and MreB (loading control) proteins were revealed using specific polyclonal antibodies on nitrocellulose membranes. In comparison with the control strain (empty vector), cells over expressing CcnA show + 35% and + 30% of CtrA in NI and I conditions, respectively. CcnA, cell cycle noncoding RNA A; WT, wild-type.

https://doi.org/10.1371/journal.pbio.3001528.g007

dependent, thus able to provide a basal level of transcription even in absence of methylation. Results clearly showed that CcnA can increase CtrA steady state levels in the Δ*ccrM* mutant closer to the WT levels. Presumably, the lower level of CtrA depends on the amount of mRNA corresponding to P2 that may be lower in the Δ*ccrM* background. Moreover, the mechanism by which CcnA increases CtrA protein levels is independent from CcrM, possibly acting on the P2 promoter.

To provide a more complete characterization of CcnA role, we combined CcnA ectopic expression (sense or antisense) with Δ*pleC*, a mutant impaired in the negative control of DivK phosphorylation level. By considering that (i) DivK~P inhibits CtrA stability and activity and (ii) that PleC is DivK's phosphatase, CtrA levels in the Δ*pleC* mutant are low (Fig 8A). Therefore, overexpression of CcnA might compensate the defects in this mutant, restoring a phenotype resembling the WT.

We introduced *ccnA* or *ccnA-as* in Δ*pleC* mutant and observed the morphology, motility in soft agar plates, sensitivity to the CbK phage, and stalk length. In agreement with our reasoning, the ectopic expression of CcnA was able to rescue Δ*pleC* defects, restoring stalks and motility while the expression of the CcnA-as caused a very severe phenotype (Fig 8B–8E). Electron microscopy was used to characterize more in details the phenotypes (Fig 8B). Results showed that upon CcnA expression (Fig 8C), stalks were longer in the Δ*pleC* background cells compared to WT cells (Fig 8D) and motility was also partially restored (Fig 8E). On the contrary, the expression of the antisense induced a severe growth and morphological phenotype with absence of polar structures in the majority of cells (Fig 8C and 8D).

We asked whether this suppression was just obtained by increasing the level of CtrA or if it was also able to affect the phosphorylation and, therefore, the activity of CtrA. We measured CtrA~P by Phos-Tag technique (S15 Fig). This analysis revealed that the CcnA expression was indeed able to increase protein levels of CtrA and slightly CtrA~P in Δ*pleC*.

Finally, we measured the sensitivity of *C. crescentus* to the phage CbK, which is adsorbed by the flagellum and enters the cells by attachment to the pili structures (Fig 8F). As the main subunit PilA of the pilus is completely under the control of CtrA, a *ΔpleC* mutant has an unfunctional flagellum and no pili, making this strain resistant to CbK infection [56,57]. Results showed that the expression of CcnA was able to completely restore the sensitivity of *C. crescentus* to CbK to WT levels, suggesting a de novo synthesis of the pili. The expression of CcnA-as did not change the resistance to the phage infection of the Δ*pleC* mutant, as shown by phage-induced lysis (Fig 8F).

Conservation of CcnA in the class *Alphaproteobacteria*

Considering the key role of CcnA in *C. crescentus* coordinating CtrA and GcrA, two of the principal master regulators of cell cycle, we asked whether its function was conserved in bacteria that share the regulatory mechanisms by those master regulators. We considered a well-known bacterial model, *S. meliloti*, a symbiotic nitrogen-fixing organism. *S. meliloti* shares with *C. crescentus* most of the regulatory circuit driving cell cycle, including CtrA [40,60]. Therefore, we took advantage of the expression system we used for *C. crescentus*, which is compatible with expression in *S. meliloti* [36]. Expressing *C. crescentus* CcnA in *S. meliloti* slowed growth and caused an abnormal cellular morphology (S16A Fig) in comparison with the same vector expressing the empty plasmid. We therefore asked whether this alteration in cell morphology was due to a change in CtrA steady state levels (S16B Fig). Indeed, the overexpression of *ccnA* in *S. meliloti* cells showed an increase of CtrA proteins levels in comparison with the strain containing the empty vector, suggesting a similar mechanism than *C. crescentus*. Results showed that CcnA of *C. crescentus* is able to induce a cell cycle defect, which is branched cells

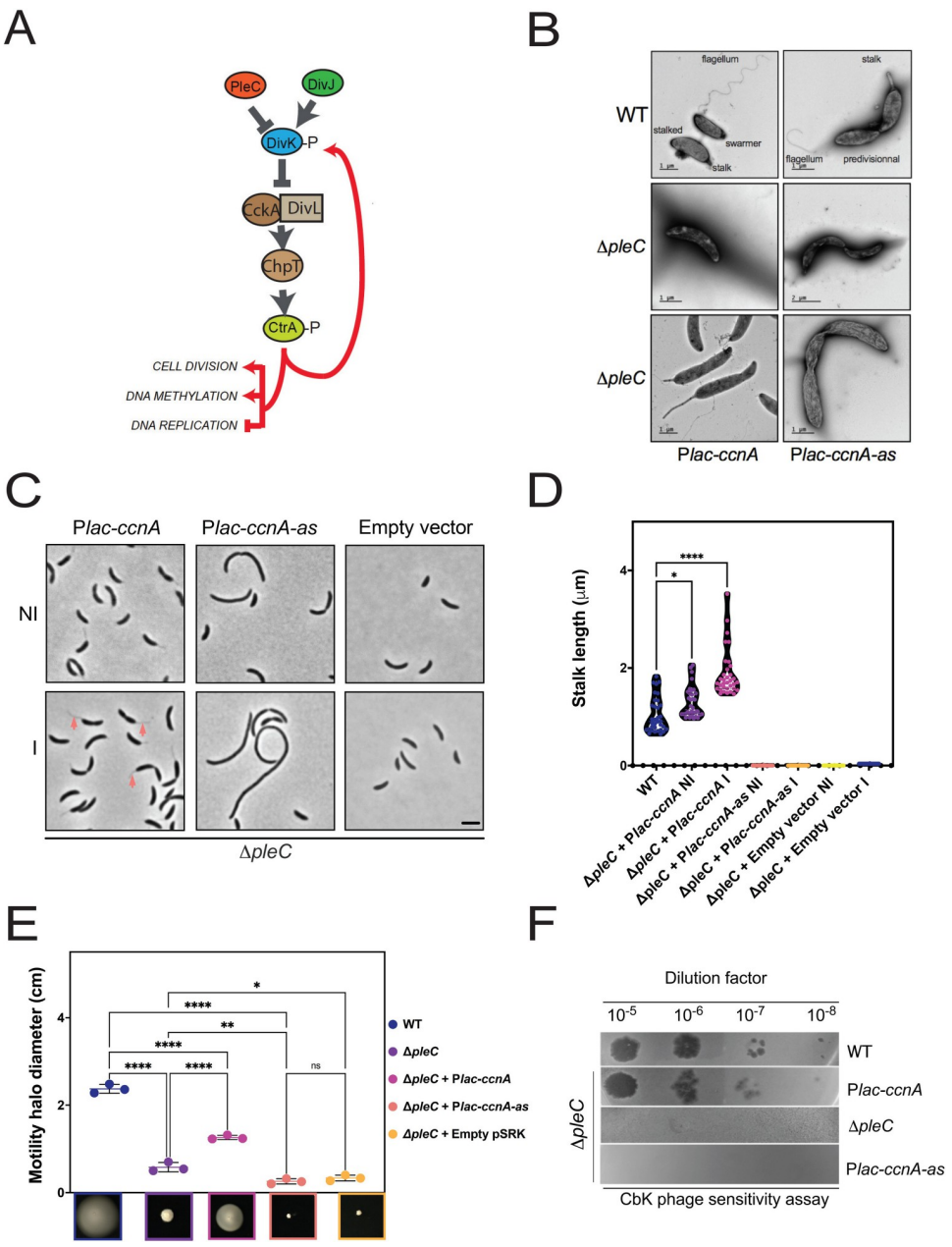

Fig 8. CcnA rescues the pleiotropic phenotypes of Δ*pleC*. **(A)** Schematic representation of CtrA-DivK negative feedback loop in *C. crescentus*. DivK phosphorylation level is controlled by its kinase DivJ and its phosphatase PleC. At the swarmer cell pole, DivK must be dephosphorylated in order to enable the phosphorelay CckA-ChpT-CtrA. At the stalk pole, the presence of DivJ/absence of PleC keeps DivK fully phosphorylated, leading to a block of CckA scaffold DivL. The absence of PleC causes a decrease of CtrA [58], both at the phosphorylation and protein levels as CtrA-P controls its own transcription from the promoter P2. **(B)** Electron microscopy images of WT cells, Δ*pleC* cells, and Δ*pleC* cells carrying either P*lac-ccnA* or P*lac-ccnA-as* cells grown in PYE without IPTG at 30˚C until OD_{600nm} = 0.6. **(C)** Phase contrast images of Δ*pleC* cells carrying a plasmid with *ccnA* or its antisense *ccnA-as* under the control of a *Plac* promoter (Δ*pleC*+ P*lac-ccnA* or Δ*pleC*+ P*lac-ccnA-as*) or Δ*pleC* cells carrying an empty vector (Δ*pleC*+ empty vector) grown in PYE at 30˚C until OD_{600nm} = 0.6. Induction of *ccnA* or *ccnA-as* was made when cells reached 0.6 by the addition of IPTG 1 mM for 30 min. Scale bar = 2 μm. **(D)** Violin plots of stalks length per cell for each strain tested in Fig 8C plus a WT *C. crescentus* as a control for normal stalk length. Stalk length was measured by using BacStalk software [59]. Statistical significance was determined using ANOVA with Brown–Forsythe and Welch's tests with a Dunnett's T3 multiple comparisons test. *: p.val = 0.0117; ****: p.val < 0.0001. Raw data are in S5 Table. **(E) Swarming assay on 0.25% soft agar plates.** A volume of 1 μL of each culture from cultures of Fig 8C was deposited into the PYE soft agar and incubated at 30˚C for 5 to 6 d. *N* = 3. The diameter in cm of each mobility halo was measured with Fiji

and reported in S4 Table. Statistical significance was determined using ANOVA with Šídák's multiple comparisons test. ns, difference not significant, *: p.val = 0.0242, **: p.val = 0.0039, ****: p.val < 0.0001. Data are in S9 Table. (**E**) **CbK phage sensitivity assay**. A bacterial layer of cultures from WT, Δ*pleC* + *ccnA*, Δ*pleC*, or Δ*pleC* + *ccnA-as* was deposited into a PYE-Agar plate and incubated at 30˚C. CbK phages were serially diluted (10^{0}–10^{-8}), and 4.5 μL of each phage dilution were spotted on top of the cultures and incubated at 30˚C to visualize cells lysis. WT and Δ*pleC* cells were used as a control of the presence or absence of lysis, respectively. CcnA, cell cycle noncoding RNA A; CtrA-P, CtrA phosphorylated; WT, wild-type.

https://doi.org/10.1371/journal.pbio.3001528.g008

and a clear cell division retard, similar to that observed in a delta-*divJ* mutant [40] and presumably linked to an increased level of CtrA.

The activity of *C. crescentus* CcnA in these 2 alphaproteobacterial species suggested that a putative homologous gene should be present in *S. meliloti*. We therefore scanned the genomes of the alphaproteobacterial species using GLASSgo [61] aiming to find CcnA homologs. We found a conservation of CcnA in several closely related species (S16C Fig). As expected CcnA has closer homologs in the *Caulobacterales*, but it can also be found in the other families except for the *Rickettsiales*. Considering that *Rickettsiae* have experienced a massive reduction of the genome, it is reasonable to speculate that CcnA may be a conserved factor that has coevolved with CtrA, participating in the ancestors to its regulation of transcription. Taken together, these results prompted us to compare 5′ UTRs of *ctrA* in these 2 organisms in order to find shared motifs potentially complementary to CcnA sequence and in conclusion involved in *ctrA* translation. By using an in silico analysis made with the Clustal Omega software (Madeira and colleagues, 2019), we found that the stretch of GGGG putatively interacting with CCCC of CcnA within its Loop A is conserved in the *ctrA* 5′ UTR of *S. meliloti* separated from the start codon by 6 nucleotides instead of 3 for *C. crescentus* CcnA (S16D Fig). This may explain why CcnA from *C. crescentus* is able to increase CtrA protein level in this species, even if a "CcnA-like" homolog was not clearly detected in *S. meliloti*.

Discussion

The origin of replication of *C. crescentus* is necessary for replication of the chromosome and therefore represents one of the most important regions of the genome. CtrA binding sites at the origin of replication play an inhibitory role on the replication of DNA as they allow CtrA~P to compete out the binding of DnaA [44]. Transcriptomic data indicated that some parts were nonetheless transcribed; in particular, a short gene was found transcribed (CCNA_R0094), corresponding to an essential genome region highlighted by the analysis of TnSeq data [32,41,62]. This gene is surrounded by CtrA boxes at −23 bp from the TSS and at the very end of the gene [33]. In the process of understanding the role of this ncRNA, belonging to the origin of replication, named here CcnA, we found that CcnA is a regulator of cell cycle, specifically linked to 2 master regulators, CtrA and GcrA. To the best of our knowledge, this is one of the first demonstrations of a ncRNA playing a stress-independent role in the cell cycle regulation of a bacterium. Examples of regulatory ncRNAs controlling key cellular functions can be found elsewhere in addition to the nowadays classical RyhB pathways controlling iron utilization in *E. coli*, such as the Qrr ncRNAs in *Vibrio* species, that participate in quorum sensing, or NfiS, a positive regulator of the nitrogenase in *Pseudomonas stutzeri* A1501 [63], which is folded into a compact structure that acts on the mRNA of *nifK*, encoding the β-subunit of the MoFe protein of the nitrogenase enzymatic complex, enhancing its translation.

Using qRT-PCR, we clearly showed that CcnA starts accumulating in the second half of the S-phase, coincidentally with the accumulation of CtrA, presumably as an effect of *ctrA* transcription from its promoter P1. Using several approaches, we hypothesized that expression of *ccnA* depends on cell cycle, presumably by CtrA. We also found that once CcnA starts to

accumulate, it binds the mRNA of *ctrA* by base pairing using at least one region belonging to a loop predicted to exist in its structure (Fig 4C). In vitro probing experiments on *ctrA* and *gcrA* 5′ UTRs showed that a stretch of CCCC is particularly important for CcnA to interact with its target mRNAs, possibly stabilizing the interactions. We hypothesize that this binding of CcnA on the *ctrA* 5′ UTR frees the RBS enabling translation at higher rates and therefore causes an increase in the protein levels. We predicted the structure of the 5′ UTR starting from the TSS of promoter P2 of the gene *ctrA* and it appears evident that the mRNA of *ctrA* has its putative Shine–Dalgarno (SD) of the RBS at −6 from ATG sequestered in a stem (Fig 9A). Although classically, ncRNAs pairing at the SD induce translational block, which is in disagreement with our observations, probing revealed another region of the *ctrA* mRNA that is impacted in presence of CcnA (Fig 4A), which is more compatible with a positive regulation of *ctrA* translation by CcnA. It has already been shown that a pairing of a ncRNA at the beginning of the coding sequence can have an activating role [64]. Hence, we can imagine that both binding are important and both responsible for the role of CcnA on *ctrA*. We attempted to construct a CcnA mutant corresponding to this second interaction. Unfortunately, the introduction of this mutation in CcnA makes the RNA unstable. Future studies on the structure of the *ctrA* 5′ UTR and CcnA may help elucidating this unorthodox positive mechanism of activation.

An intriguing question about CcnA is its functional relationship with the origin of replication. Why does *ccnA* belong to the origin of replication? It is fascinating to speculate that *ccnA* belongs to the *CORI* as it must be fired at low levels of CtrA~P, therefore "using" high affinity CtrA binding sites [42]. This allows the presence of CcnA when the second mRNA of *ctrA*, generated from the P2 promoter, starts accumulating. CcnA may be potentially involved in the translation of P2 mRNA of *ctrA* and therefore may act as a cell cycle timer through CtrA activation [66].

Indeed, CcnA plays a role in the regulation of the expression of CtrA as a putative activator of translation. In our model (Fig 9B and 9C), the regulatory circuit created by CtrA-CcnA and back to CtrA represents a positive feedback loop in which the regulatory layer controlled by CcnA acts on top of a second layer of transcriptional auto-activation of *ctrA* on its second strong promoter P2. In parallel, CtrA has a potential inhibitory activity on *gcrA*, creating a negative feedback loop in which GcrA activates *ctrA*, which, in turn, blocks *gcrA*. CcnA acts as well on this feedback reinforcing a reduction of translation by direct binding onto the 5′ UTR of *gcrA*. Therefore, CcnA does not create new connections between master regulators of cell cycle but in fact acts on a preexisting circuit, presumably increasing the robustness of the system. This behavior by ncRNAs has been described before [67–69]. The role of ncRNAs is therefore to consolidate the robustness of transcriptional circuits by introducing a fast post-transcriptional control on the mRNAs produced by transcription factors. From this point of view, CcnA may indeed act as key trigger for protein production linking transcription to translation. The importance of CcnA emerges when redundant mechanisms of CtrA control are not present, such as the absence of CcrM (primary activator of CtrA expression in the second half of S-phase). In all systems investigated so far, ncRNA-mediated regulations introduce a rich variety of dynamical responses, but these have mainly been studied in the case of negative regulation by the ncRNA on the target transcript. Among the peculiarities of ncRNA-mediated negative regulation in bacteria, previous studies have observed a threshold linear response of target abundance and the possibility of an ultrasensitive response in target abundance as a function of the relative transcription rate of the ncRNA and the target [30,31]. Moreover, ncRNAs may act as a fine-tuning of the affinity for different targets, but their effects might also create, in complex networks, phenomena such as bistability and oscillations [70].

Is this CcnA-dependent mechanism, controlled by CtrA itself, also conserved in organisms in which CtrA regulates the cell cycle? We studied *C. crescentus* CcnA in *S. meliloti*, where the

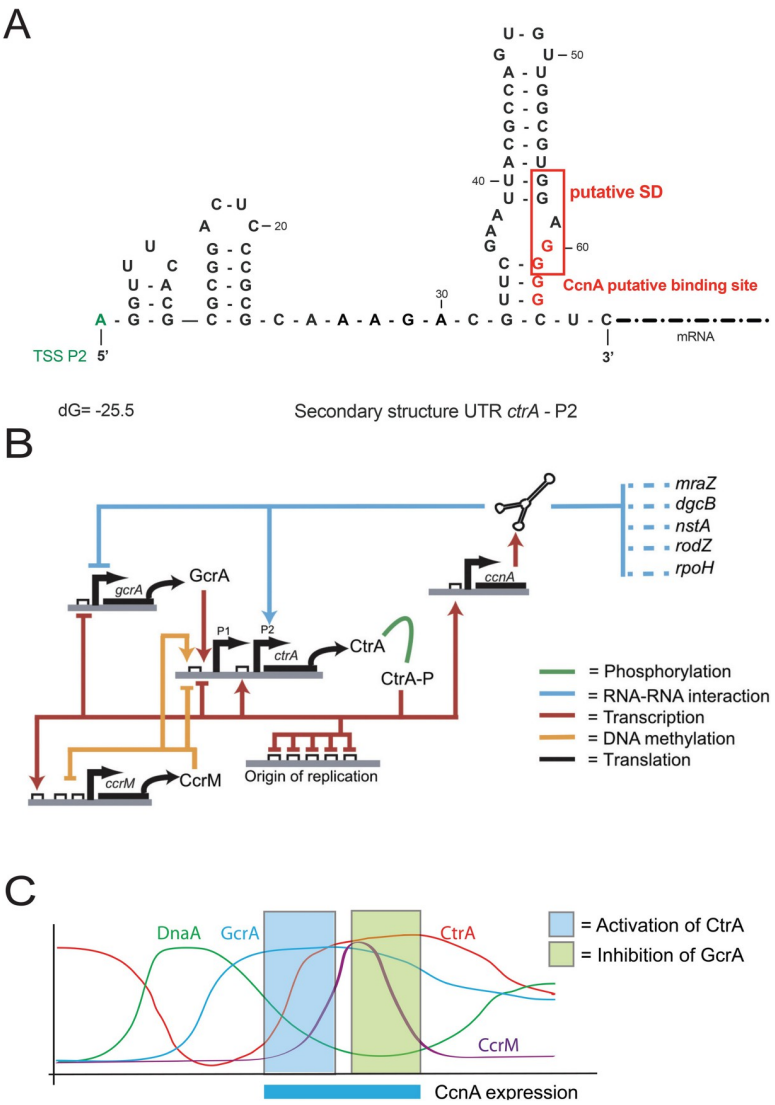

Fig 9. Integration of CcnA in the cell cycle regulation model in *C. crescentus*. **(A)** Secondary structure prediction of 5′ UTR of *ctrA* starting from the TSS of *ctrA*-P2 using « The DINAmelt Web server » –Two-state melting (folding) with default parameters for RNA energy rules [65]. The predicted free energy of the thermodynamic ensemble is −25.5 kcal/mol. "GGAGG" *ctrA*-P2 RBS is framed in red and appears to be blocked in a stem loop. Binding site of CcnA Loop A is indicated in red. **(B)** Throughout the cell cycle, the cascade of transcriptional activation of the gene *ctrA* involving GcrA and CcrM activates *ctrA*-P1 expression leading to its first protein accumulation. After the translation and activation by phosphorylation of CtrA, CtrA~P will reach the origin of replication to inhibit DNA replication. Our work suggests that simultaneously CtrA~P is potentially responsible of *ccnA* transcription. CcnA in return will create a positive feedback loop on CtrA protein accumulation after its P2 expression. This suggests that CcnA may be a key element of the second strong CtrA accumulation during the cell cycle. CcnA may also be a « CtrA-activity » modulator as its other putative targets belongs to the CtrA regulon. Concomitantly, CcnA regulates negatively putatively the translation of *gcrA* mRNA leading to a decrease of GcrA and presumably a correct and precise shut ON or OFF of the 2 master regulators. CcnA cell cycle expression window correlated in space and time with the activation and inhibition of CtrA and GcrA, respectively. **(C)** CcnA is proposed to act negatively on *gcrA* mRNA translation avoiding a de novo transcription of *ctrA-P1* and at the same time positively on *ctrA*-P2 mRNA translation to regulate the second wave of CtrA activation necessary for the expression of genes involved in fundamental processes such as cell division, chemotaxis, DNA methylation, and biogenesis of polar structures. CcnA, cell cycle noncoding RNA A; RBS, ribosome-binding site; TSS, transcriptional start site; 5′ UTR, 5′ untranslated region.

https://doi.org/10.1371/journal.pbio.3001528.g009

role of CtrA has been investigated [40,60]. In these 2 organisms, CtrA is essential and controls key cell cycle functions such as cell division and DNA replication. Consistently with our hypothesis, the expression of *C. crescentus* CcnA causes the same molecular alterations as described here in *C. crescentus*. Although more molecular investigation of homologous ncRNA in other organisms must be explored, we can hypothesize that CcnA activity may be a conserved mechanism of the regulation of the cell cycle. This new system of complex regulatory circuits carried out by CcnA indeed expand the key role of ncRNAs in bacteria, opening a new activity that will need a thorough molecular investigation of mechanistic activity of this ncRNA. The CcnA structure and consequent activity may be a new class of ncRNAs whose role is still at its beginning of study. Interestingly, a prediction of target genes among several homologs have revealed that targets usually fall into the chemotaxis and motility classes of genes, suggesting a common function. This is not surprising considering that CtrA itself is considered, in *C. crescentus* and most of alphaproteobacterial species, as a regulator of motility [33,71].

In conclusion, the regulatory mechanism centered on CcnA represents an archetype of regulatory architecture. CtrA autoregulates itself via its promoter P2 and inhibits the expression of GcrA via its binding site on the promoter region of *gcrA*. The same 2 connections are performed by CcnA that activates CtrA translation and inhibits GcrA expression. This module on top of a more classical transcriptional regulation presumably ensures a strong effect during cell cycle. Taking advantage of the simplicity of this bacterial system, more specific experiments must be performed in order to elucidate this network behavior.

Materials and methods

Strains, growth conditions, and molecular biology techniques

Strains used in this work are listed in S3 Table. *C. crescentus* strains were routinely cultured in peptone-yeast extract (PYE) medium with appropriate amount of antibiotics (Solid: Kanamycin 25 μg/ml, Tetracycline 2 μg/ml, Spectinomycin 100 μg/ml) (Liquid: Kanamycin 5 μg/ml, Tetracycline 1 μg/ml, Spectinomycin 25 μg/ml) and 0.3% xylose or 0.2% glucose whenever necessary. *S. meliloti* strains were cultured in tryptone-yeast (TY) extract medium with appropriate antibiotics (Streptomycin 500 μg/ml, Kanamycin 200 μg/ml). *E. coli* was grown in lysogeny broth (LB) medium. The cultures were grown at 30˚C or 37˚C as required for different experiments. Synchronization of the *C. crescentus* cells was done using Percoll or Ludox as described before [72]. *E. coli* strains were grown at 37˚C in LB or solid medium with required amount of antibiotic supplements (Ampicillin 100 μg/ml, Kanamycin 50 μg/ml, Tetracycline 10 μg/ml) as necessary. *C. crescentus* cells were transformed with different plasmids by electroporation. Western blotting was performed as previously described [60] using antibodies against CtrA, DnaA, GcrA, and MreB using 1:5,000 dilutions. Bands were quantified using ImageJ [73]. pSRK vectors were constructed as previously described using primers listed in S3 Table amplified using the polymerase Q5 (NEB). Soft agar plates were prepared with 0.25% agar; images were taken using an IC-Capture Camera at 75% of magnification. Phostag was performed as previously described [60]. CbK phage sensitivity assay was also performed as previously described [56].

MS2-affinity purification coupled with RNA sequencing

Strains containing MS2-CcnA and MS2 UTRs of *ctrA* P1 and P2 were induced by 1 mM IPTG for 30 min harvested and used to perform MAPS as previously described [74]. Analysis was performed by the following protocol. Reads were mapped to the indexed *C. crescentus* NA1000 genome (NC_011916) with Bowtie2 (Langmead and colleagues, 2018) by using the following

command: "bowtie2—qc-filter—threads 18—no-mixed—mp 10—no-discordant -x NA1000—passthrough -1 R1_001.fastq.gz -2 R2_001.fastq.gz", which only returns concordant alignments in the form of *innies* (mates face each other) with at least 10 of MAPQ score. As we wanted to align reads that also fall outside coding sequences, we first mapped on the genome and then we used genome regions defined as explained below to calculate the coverage of the regions. In doing so, we need to consider that the paired libraries were obtained by using a stranded protocol (Illumina). For this reason, we first split the genome alignments into 2 files, one containing all pairs assigned with the flag 99/147 and the other reads pairs with flag 83/163. Basically, in doing so, we are putting all pairs aligned on the genome with a certain orientation in one file and all those aligned in reverse orientation in another. Each file is used as input to BamCoverage (Ramirez and colleagues, 2016) to calculate coverage in 1 nt bins of the genome. At this point, we used several files containing genome region coordinates (described below) to calculate the coverage of the regions, by taking reads on the basis of the expected alignment orientation with the transcript. For instance, when considering CDS, we will proceed similarly to what is done in standard RNAseq, i.e., we will calculate the coverage of the CDS by summing all the genome coverage values that fall within the CDS in the expected orientation. In this way, we were able to calculate the coverage of predefined regions that are not present in the annotation file (i.e., the gff) of the NA1000 genome. Once obtained the coverage for our regions, we analyzed them independently, by calculating a log2 ratio of the normalized coverage in the MS-purified sample and the control. We defined as candidate targets for CcnA all genes for which one of the regions have a log2 ratio of the coverage of at least 2 (4-fold increase) using the RPM-transformed data. To avoid artifacts for small coverage values that are subject to high experimental fluctuations, we also ask that each region has a coverage larger than the lower 25% of the regions in the MS experiment.

Most tools developed to calculate sequencing coverage from RNAseq data usually rely on a preexisting genome annotation, and among all features encoded in that file, they often focus on "CDS" or "gene". This can have problems, as, for instance, ncRNAs do not have a CDS associated, and, therefore, tools strictly using CDS coordinates will completely overlook ncRNAs. In the present context, we were interested in understanding if MAPS data might allow inference about more detailed questions concerning a ncRNA target transcript. For instance, if we can get information on the specific region of the transcript that is bound by the ncRNA under examination. Together with defining a list of potentially bound transcripts in the different MAPS experiments performed in this work, we also defined 5′ and 3′ UTRs for each gene and analyzed the coverage of the 3 regions independently. The 5′ UTR of a gene was defined on the basis of the experimentally determined transcription starts sites from Zhou and colleagues if the gene was present in their data, else as the 100 nt region upstream of the gene. Similarly, to avoid considering short UTRs, if the UTR defined by Zhou and colleagues was less than 100 nt, we define the 5′ UTR as the 100-nucleotide region preceding the start of the CDS or ncRNA. As there is no similar experimental data for 3′ UTRs, we arbitrarily defined these regions as the 250 nucleotides going from 50 nt within the CDS or ncRNA to 200 nt downstream.

Microscopy analysis

Cells were observed on a 24 × 50 mm coverslip under a 0.15% agarose-PYE "pad" to immobilize the cells. Samples were observed, thanks to an epifluorescent-inverted microscope Nikon Eclipse TiE E PFS (100 × oil objective NA 1.45 Phase Contrast). Cells morphologies and fluorescent images were analyzed using ImageJ and MicrobeJ [37,73]. Stalk length was measured by using BacStalk software [75]. Electron microscopy (EM) was performed by placing 5 μL

drops of the bacteria suspension for 3 min directly on glow discharged carbon coated grids (EMS). The grids were then washed with 2 drops of 2% aqueous uranyl acetate and stained with a third drop for 2 min. Grids were dried on filter paper and the samples were analyzed using a Tecnai 200KV electron microscope (FEI), and digital acquisitions were made with a numeric camera (Oneview, Gatan).

Quantitative real-time PCR for transcriptional analyses

RNAs were prepared from cultures at $OD_{600} \sim 0.6$. The cells were harvested and frozen at −80˚C. Total RNAs were isolated from the pellet using the Maxwell 16 LEV miRNA Tissue Kit (Promega) according to the manufacturer's instructions and an extra TURBO DNase (Invitrogen) digestion step to eliminate the contaminating DNA. The RNA quality was assessed by Tape station system (Agilent). RNA was quantified at 260 nm (NanoDrop 1000; Thermo Fisher Scientific). For cDNA synthesis, 1 μg total RNA and 0.5 μg random primers (Promega) were used with the GoScript Reverse transcriptase (Promega) according to the manufacturer instruction. qRT-PCR analyses were performed on a CFX96 Real-Time System (Bio-Rad). The reaction volume was 15 μL and the final concentration of each primer was 0.5 μM. The cycling parameters of the qRT-PCR were 98˚C for 2 min, followed by 45 cycles of 98˚C for 5 s, 60˚C for 10 s. A final melting curve from 65˚C to 95˚C is added to determine the specificity of the amplification. To determine the amplification kinetics of each product, the fluorescence derived from the incorporation of EvaGreen into the double-stranded PCR products was measured at the end of each cycle using the SsoFast EvaGreen Supermix 2X Kit (Bio-Rad, France). The results were analyzed using Bio-Rad CFX Maestro software, version 1.1 (Bio-Rad, France). Based on beta-galactosidase data, fusing the *ccnA* promoter with the ORF of *lacZ*, we found that CcnA transcription is high with levels around 10^4 Miller units. Therefore, the RNA16S gene (also highly expressed) was used as a reference for normalization. For each point, a technical duplicate was performed. The amplification efficiencies for each primer pairs were comprised between 80% and 100%. All primer pairs used for qRT-PCR are reported in the S3 Table.

Flow cytometry analysis

C. crescentus cells grown to exponential, stationary phase or synchronized were harvested and stored in 70% ethanol at −20˚C until further use. DNA content of cells was analyzed with flow cytometry by using the protocol as described in (Bergé and colleagues, 2020) with slight modifications.

For synchronized cultures, a population of pure G1 cells (swarmer cells) was obtained by separation with density gradient with Percoll. Briefly, cells from an overnight culture were diluted to OD = 0.1 and grown to 0.5 to 0.6, then centrifuged 5 min at 8,000*g* at 4˚C. The supernatant was removed and the pellet resuspended in 750 μL of cold 1X M2-Salt and mixed with 700 μL of cold Percoll and vortexed then centrifuged at 12,000*g* at 4˚C for 20 min. The top band (predivisional and stalk cells) was removed and the bottom band (swarmer G1 cells) was collected and washed 3 times in cold M2-Salt. The cells were then resuspended in 2 mL of prewarmed PYE (30˚C). A volume of 200 μL of samples following the cell cycle were collected every 15 min from t = 0 to t = 120 min and stored in 70% ethanol and processed as described below.

Due to the small size of the bacterium *C. crescentus*, we used a threshold and a trigger with the SSC signal (side scatter). The density plots obtained (small-angle scattering FSC versus wide angle scattering SSC signals) were gated on the population of interest, filtered to remove multiple events, and then analyzed for the fluorescence intensity (FL1 525/30 nm) of the DNA

probe SYTO 9 Green Fluorescent Nucleic Acid Stain at a final concentration of 2 μM in the buffer (10 mM Tris–HCl pH = 7.5; 1 mM EDTA; 0.01% triton X100; 50 mM Na-citrate). Proportion of cells harboring 1N, 2N, and ≥3N DNA were analyzed by gating the peaks of the Syto9 fluorescence histograms. Samples were run in the low-pressure mode (5 to 10K events/s). A total number of 300 to 500K particles were collected per sample. Data were acquired with a S3e cells sorter (Bio-Rad) using 488 and 561 nm lasers and were analyzed and plotted using FlowJo v10.6. Data are representative of 3 to 5 biological replicates, and statistical analyses were carried out with Prism.v8.2 using ANOVA test.

Probing experiments

Templates for in vitro probing, containing a T7 promoter, were obtained by PCR amplification. Lead acetate degradation and inline probing assays were performed as previously described [46]. In brief, 0.2 μM of *in vitro*–generated *gcrA+209* and P2-*ctrA+143*, 5′ end-labeled were incubated with or without 1 μM CcnA ncRNA. Radiolabeled RNA was incubated 5 min at 90˚C with alkaline buffer or 5 min at 37˚C with ribonuclease T1 (0.1 U; Ambion) to generate the Alkaline (OH) ladder and the T1 ladder, respectively. RNA was analyzed on an 8% acrylamide/7M urea gel.

RNA sequencing

Cultures were harvested at 0.6 OD_{600} and frozen in liquid nitrogen as previously described [60]. Total RNA was prepared using RNeasy Mini Kit (Qiagen). Ribosomal RNAs were removed ("depleted" samples) using the Bacterial RiboZero (Illumina), and libraries for MiSeq (V3 cassette) were prepared using the Stranded True Seq RNAseq Kit (Illumina). For the analysis of S11 Fig, reads were mapped using the Galaxy platform [76] by Bowtie2, reduced to 10 bp reads per kilobase per million mapped reads (RPKM) in a Bedgraph format by BamCoverage [77] and visualized by the Integrative Genomics Viewer (IGV) [78]. For analysis shown in S12 Fig and S2 Table, read alignments were performed with bowtie2 [79] and the following additional parameters:—no-discordant—no-mixed—no-unal–dovetail. The resulting sam file was first converted into a bam file with samtools [80] and then used as input to HTSeq count [81]. Abundance matrices for all annotated genes were assembled together after removal of tRNA and rRNA genes and used for differential gene expression analysis by using the R package DESeq2 [82]. Selection of DEGs was based on the contrast among libraries from a strain expressing the sense ncRNA CcnA and the strain expressing the corresponding antisense ncRNA by applying the following thresholds: FDR < 0.01. We did not filter at a log fold change threshold to let the DESeq2 algorithm exploits the estimation of dispersion to provide a full list of likely DEGs. This resulted in 215 DEGS, ranging in absolute value from a log fold change of 0.48 to a maximum of 2.9. Most of the DEGS are up-regulated (208, or 97% of the total). The differential gene expression analysis was integrated with a number of available information on the cell cycle of *C. crescentus*: essentiality data come from [83]; the list of genes significantly changing their expression level during the cell cycle is from [84] and are based on a RNAseq experiment comprising 5 time points during the cell cycle in triplicate; GcrA ChIP--Seq data come from [85]. We downloaded the reads corresponding to the GcrA sample and mapped them on the NA1000 genome to obtain a coverage profile. This profile was used to get an average coverage for each gene by considering the window going from 200 nt upstream of the ATG of the gene to 50 nt within the coding sequences. Data concerning the dependence of genes from methylation come from [86] and were identified on the basis of a microarray analysis of strains engineered through removal of the gene encoding the methyltransferase (*ccrM*). The presence of CtrA binding sites (full and half) is based on scanning the genome with the

PWM obtained by [87] and a threshold of 70% of the maximum score, calculated as from [87]. Moreover, a site was indicated as present for a gene if it was found in the 250 nt upstream of the ATG and a site was assigned to the closest gene. The heatmap figure was obtained with the R package Pheatmap and integrates the above annotations with gene expression data in the present work (S12 Fig). All fastQ files are available from the Dryad database (doi: 10.5061/dryad.4mw6m909k) [88].

Primer extension

Transcriptional +1 of CcnA ncRNA was determined by primer extension. Briefly, 10 μg of total RNA was incubated with 2 pmol of radiolabelled primer (EM5194) and 0.5 mM dNTPs for 5 min at 65˚C, followed by 1 min on ice. Reverse transcription was initiated by adding ProtoScript II Buffer (1×), ProtoScript II (200 units, NEB) and DTT (5 mM). The reaction mixture was incubated at 42˚C for 1 h. The enzyme was inactivated at 90˚C for 10 min. The reaction was precipitated and then migrated on a denaturing 8% polyacrylamide gel. Gel was dried, exposed to phosphor screens, and visualized using the Typhoon Trio (GE Healthcare) instrument.

Electrophoretic Mobility Shift Assays (EMSA)

EMSA were performed according to Morita and colleagues [89], with some modifications. 5′ end-radiolabeled *ctrAp2*, *ctrAp2_LoopA*, *gcrA*, or *gcrA-LoopA* was heated for 1 min at 90˚C and put on ice for 1 min. *ctrAp2* or *ctrAp2_LoopA* RNA was diluted at 5 nM in binding buffer (50 mM Tris–HCl (pH 8.0), 25 mM $MgCl_2$, 20 mM KCl, 12.5 μg/mL yeast tRNA), *gcrA* or *gcrA-LoopA* RNA was diluted at 5 nM in binding buffer II (10 mM Tris–HCl (pH 7.0), 10 mM $MgCl_2$, 1,000 mM KCl, 12.5 μg/mL yeast tRNA) and mixed with CcnA or CcnA-LoopA at different concentrations (0 to 2,000 nM). Samples were incubated for 15 min at 37˚C, and reactions were stopped by addition of 1 μL of nondenaturing loading buffer (1X TBE, 50% glycerol, 0.1% bromophenol blue, 0.1% xylene cyanol). Samples were resolved on native polyacrylamide gels (5% acrylamide:bisacrylamide 29:1) in cold TBE 1X and migrated at 50 V, at 4˚C. Gels were dried, exposed to phosphor screens, and visualized using the Typhoon Trio (GE Healthcare) instrument. Image Studio Lite software (LICOR) was used for densitometry analysis.

Data deposited in the Dryad repository: https://doi.org/10.5061/dryad.4mw6m909k [88].

Supporting information

S1 Table. MAPS and reverse MAPS targets.
(XLSX)

S2 Table. RNAseq of strains overexpressing *ccnA* and *ccnA-as*.
(XLSX)

S3 Table. Strains and primers used in this work.
(XLSX)

S4 Table. Diameters of halos cited in Figs 7 and 8.
(XLSX)

S5 Table. Stalk length measurement by BacStalk software cited in Figs 8 and S3.
(XLSX)

S6 Table. RNAseq Rockhopper data cited in S1A Fig.
(XLSX)

S7 Table. Raw data of growth curves cited in Figs 2, 6, S8, and S9.
(XLSX)

S8 Table. Raw data of cell length and width measurements obtained by MicrobeJ cited in Figs 2, 7, 8, S3, S8, and S14.
(XLSX)

S9 Table. Raw data of remaining figures.
(XLSX)

S1 Fig. (A) Transcription levels of CcnA in a CtrA thermosensitive strain (*ctrAts*). WT cells were grown in PYE until OD_{600nm} = 0.6, and *ctrA-ts* cells were grown in PYE until OD_{600nm} = 0.6 and kept for 1 h at the permissive temperature 30˚ C or shifted 1 h to the restrictive temperature 37˚C. Total RNA was extracted in each condition and prepared for RNAseq. Data were analyzed using Rockhopper [90,91] with the following parameters: strand specific, paired end, verbose output (generation of raw and normalized counts for each transcripts and RPKM value). Statistical analysis was performed using Kruskal–Wallis test with a Dunn's multiple comparisons test (Prism GraphPad 9.1.2), and results are shown as mean (*N* = 3) of normalized counts +/− SD, ns, difference not significant, * = p.val = 0.0225. Raw data are provided in S6 Table. **(B)** Expression level of CcnA in *C. crescentus* strains carrying *ccnA* and *ccnA-as* in a pSRK plasmid with or without induction by addition of IPTG 1 mM 30 min (related to Figs 1 and S9) and in different backgrounds (WT, Δ*cpdR*, Δ*rcdA*, Δ*popA*, Δ*divJ*, and Δ*prom*). Cells were grown in PYE at 30˚C, then the expression of *ccnA* was determined by qRT-PCR and compared to 16S level. Results are presented as mean (*N* = 3) +/− SD. **(C)** WT *C. crescentus* cells, or *C. crescentus* cells deleted from the genes *cpdR (ΔcpdR)*, *rcdA (ΔrcdA)*, or *popA (ΔpopA)*, belonging to the proteolysis machinery ClpXP of *C. crescentus*, were grown in PYE at 30˚C until OD_{600nm} = 0.6. Proteins were extracted and separated on a SDS-PAGE gel for Western blotting. CtrA and MreB (loading control) were revealed using specific polyclonal antibodies on nitrocellulose membranes. CcnA, cell cycle noncoding RNA A; PYE, peptone yeast extract; qRT-PCR, quantitative real-time PCR; RNAseq, RNA sequencing; RPKM, reads per kilobase per million mapped reads; WT, wild-type.
(TIF)

S2 Fig. (A) Determination of the transcriptional +1 site of CcnA by primer extension related to Figs 1 and 5. Total RNA extracted from WT cells or containing P*lac-ccnA and* P*lac-ccnA-Loop A* were used with radiolabelled oligo. The reaction was done with (+) or without (−) reverse transcriptase. The same oligo was used for *ccnA* sequencing (GCAT). The +1 signal is represented by the arrow. **(B) Mutation of the *ctrA* mRNA ($ctrA_{CCCC}$) and ncRNA CcnA binding site.** Solid lines indicate CcnA binding sites on *ctrA*. Boxed gray text corresponds to the nucleotides mutated. The translation start codon is shown in bold. P2-$ctrA_{CCCC}$ (+143 nt from the P2-*ctrA* promoter) 5 nM RNA fragment was incubated with increasing concentration of CcnA (bottom). Data represent the mean of 2 independent experiments. **(C) Mutation of the *gcrA* mRNA ($gcrA_{CCCC}$) and ncRNA CcnA binding site**. Solid lines indicate CcnA binding sites on *gcrA*. Boxed gray text corresponds to the nucleotides mutated. $gcrA_{CCCC}$ 5 nM RNA fragment was incubated with increasing concentration of CcnA (bottom). Data represent 2 independent experiments. CcnA, cell cycle noncoding RNA A; ncRNA, noncoding RNA; WT, wild-type.
(TIF)

S3 Fig. Violin plots of stalks length per cell for a WT + P*lac-ccnA* strain tested in Fig 2D compared to a WT *C. crescentus* used as a control for normal stalk length (same as 8D). Stalk length was measured by using BacStalk software [59]. Statistical significance was determined using an unpaired *t* test with Welch's correction for different SD. ****: p.val < 0.0001. Raw data are in S5 Table. WT, wild-type.
(TIF)

S4 Fig. (**A**) Flow cytometry profiles after SYTO 9 staining showing DNA content of WT cells, WT cells carrying either an empty pSRK (empty vector) or *ccnA* under the control of a P*lac* promoter (P*lac-ccnA*) grown in PYE until $OD_{600nm} = 0.6$. Then, induction of P*lac-ccnA* was made by addition of IPTG 10 mM overnight. A total number of 300,000 particles were analyzed per sample by flow cytometry. (**B**) Proportions of cells harboring 1N, 2N, and $\geq$3N DNA in the population were analyzed by gating the histograms in (B). Data are representative of 3 biological replicates. Statistical analyses were carried out using ANOVA Tukey test. ns, difference not significant, ***: p.val. < 0.001. PYE, peptone yeast extract; WT, wild-type.
(TIF)

S5 Fig. (**A**) Schematic of the CckA-ChpT-CtrA phosphorelay. CckA is a hybrid histidine kinase; at the swarmer cell, it acts as a kinase and at the stalked cell pole as a phosphatase. CckA autophosphorylates, then transphosphorylates the histidine phosphotransferase ChpT that, in return, transphosphorylates CtrA and CtrA proteolysis adapter protein CpdR. (**B**) WT cells carrying either an empty pSRK (empty vector) or *ccnA* under the control of a P*lac* promoter (*Plac-ccnA*) were grown in PYE at 30˚C until $OD_{600nm} = 0.6$. Then, the induction of P*lac-ccnA* was made by addition of IPTG 1 mM 30 min. Proteins were extracted and separated on a SDS-PAGE containing Phostag and Mn^{2+} to visualize CtrA phosphorylation level. CtrA was revealed using specific polyclonal antibodies on nitrocellulose membrane. In comparison with the control strain (empty vector), cells overexpressing CcnA show + 85% and + 45% in NI and I conditions, respectively. (**C**) Phase contrast and epifluorescence images of P*chpT-chpT*::*yfp* cells carrying *ccnA* (*Plac-ccnA*) or an empty pSRK (empty vector) grown in PYE at 30˚C until $OD_{600nm} = 0.6$. Scale bar = 2 μm. (**D**) Histograms showing quantification of ChpT-YFP signal in P*chpT-chpT*::*yfp* cells carrying P*lac-ccnA* or an empty vector by using MicrobeJ. Results are shown as fraction of total cells with absence of cluster, presence of cluster, and presence of high-intensity cluster. At least 1,000 cells were analyzed for each condition. Data are in S9 Table. (**E**) Histograms showing morphologies typology of cells related to S5C and S5D with detected cluster using MicrobeJ software [37]. Data are in S9 Table. (**F**) P*chpT-chpT*::*yfp* cells carrying either an empty vector or P*lac-ccnA* were grown in PYE 30˚C until $OD_{600} = 0.6$. Then, the induction of P*lac-ccnA* was made by addition of IPTG 1 mM 30 min. Proteins were extracted and separated on a SDS-PAGE for Western blotting. GFP and MreB (loading control) were revealed using specific polyclonal antibodies on nitrocellulose membrane. PYE, peptone yeast extract; WT, wild-type.
(TIF)

S6 Fig. Schematic representation of the strategy used to study *ccnA* down-regulation phenotypes without lethality. Our only viable deletion obtained in this study was a 45-bp long deletion comprising the CtrA box located within the promoter region of *ccnA*. Attempts to delete the *ccnA* gene sequence could not be constructed.
(TIF)

S7 Fig. (**A**) **Determination of the transcriptional +1 site of CcnA ncRNA by primer extension.** Total RNA extracted from WT cells, deleted *ccnA* promoter (*Δprom*), and containing P*ccnA-ccnA* (Δ*prom* + P*ccnA-ccnA*) was used with radiolabelled oligo. The reaction was done

with (+) or without (−) reverse transcriptase. The same oligo was used for *ccnA* sequencing (GCAT). The sequence is presented as the reverse complement. The +1 signal is represented by the arrow. (**B)** WT cells, Δ*prom* cells, Δ*prom* cells carrying either an empty pMR10 low-copy plasmid (Δ*prom* + *empty vector)* or harboring *ccnA* under the control of its own promoter (Δ*prom* + P*ccnA-ccnA)* were grown in PYE at 30˚C until OD_{600nm} = 0.6. Proteins were extracted and separated on a SDS-PAGE for western blotting. CtrA and MreB (loading control) were revealed using specific polyclonal antibodies on nitrocellulose membranes. CcnA, cell cycle noncoding RNA A; ncRNA, noncoding RNA; PYE, peptone yeast extract; WT, wild-type.
(TIF)

S8 Fig. (**A)** Phase contrast images of WT cells, Δ*prom* cells, Δ*prom* cells carrying *ccnA* under the control of its own promoter in a pMR10 low-copy plasmid (Δ*prom* + P*ccnA-ccnA)*, WT cells carrying an empty low-copy plasmid pMR10 (WT + empty vector) or Δ*prom* cells carrying an empty low-copy plasmid pMR10 (Δ*prom* + empty vector) grown overnight in PYE at 30˚C until OD_{600nm} = 0.6. Scale bar corresponds to 2 μm. Cells were analyzed using MicrobeJ [92] to assess cell length. Approximately 422 cells were analyzed. Statistical significance was determined using ANOVA with Tukey multiple comparisons test. ns, difference not significant ***: p.val = 0.0001 and ****: p.val < 0.0001. Raw data are provided in S8 Table. (**B) Growth curves of Δ*prom* cells complemented with *ccnA***. WT cells carrying an empty low-copy plasmid pMR10 (WT + empty vector), Δ*prom* cells carrying either *ccnA* under the control of its own promoter in a pMR10 low-copy plasmid (Δ*prom* + P*ccnA-ccnA)* or an empty low-copy plasmid pMR10 (Δ*prom* + empty vector) were grown overnight in PYE. A volume of 200 μL of cells back-diluted from stationary phase cultures to an OD_{600nm} = 0.02 were then grown on 96 wells in PYE at 30˚C. Cell growth was monitored overnight with a Spark-TM at 30˚C and a shaking (orbital) amplitude of 6 mm and a shaking (orbital) frequency of 96 rpm. Results are shown as mean *N* = 2 biological with 3 technical replicates per biological replicates. Raw data are provided in S7 Table. PYE, peptone yeast extract; WT, wild-type.
(TIF)

S9 Fig. (A) WT cells, WT cells carrying either an empty pSRK (empty vector) or *ccnA-as* under the control of a P*lac* promoter (P*lac-ccnA-as*) were grown in PYE at 30˚C until OD_{600nm} = 0.6. Then, the induction of P*lac-ccnA-as* was made by addition of IPTG 1 mM 30 min. As a control of induction, WT cells carrying an empty vector were also incubated 30 min in presence of IPTG 1 mM and WT cells with no induction were used as a control. Δ*prom* cells were used as a comparison for CtrA levels. Proteins were extracted and separated on a SDS-PAGE gel for western blotting. CtrA and MreB (loading control) proteins were revealed using specific polyclonal antibodies on nitrocellulose membranes. (**B)** Flow cytometry profiles after SYTO 9 staining showing DNA content of WT cells, WT cells carrying either an empty pSRK (empty vector) or *ccnA-as* under the control of a *Plac* promoter (P*lac-ccnA-as*) grown in PYE until OD_{600nm} = 0.6. Then, induction of P*lac-ccnA-as* was made by addition of IPTG 1 mM 1 h 30 min. A total number of 300,000 particles were analyzed per sample by flow cytometry. (**C)** Proportions of cells harboring 1N, 2N, and ≥3N DNA in the population were analyzed by gating the histograms in (C). Data are representative of 3 biological replicates. Sstatistical analyses were carried out using ANOVA Tukey test. ****: p.val < 0.0001. Data are in S9 Table. (**D) Growth curves following the expression of CcnA antisense (P*lac-ccnA-as*).** WT cells and WT cells carrying either an empty pSRK (empty vector) or a pSRK with *ccnA* under the control of an inducible P*lac* promoter *(Plac-ccnA)* or P*lac-ccnA-as* were grown overnight in PYE without IPTG. A volume of 200 μL of cells back-diluted from stationary phase cultures to an OD_{600nm} = 0.02 were grown on 96 wells in PYE supplemented with 1 mM IPTG. Cell growth

was monitored overnight with a Spark-TM at 30˚C and a shaking (orbital) amplitude of 6 mm and a shaking (orbital) frequency of 96 rpm. Doubling time of P*lac-ccnA-as* cells equals to 201.96 min +/− 11.66 with 1 mM IPTG. Results are shown as mean $N = 3$ biological with 3 technical replicates. Raw data are provided in S7 Table. PYE, peptone yeast extract; WT, wild-type.
(TIF)

S10 Fig. Schematic of the MAPS technique. MAPS consists of the fusion of a ncRNA of interest, here CcnA, with an RNA aptamer called MS2 [74]. In this technique, the protein MS2 is used for its high affinity to the RNA MS2 from the bacteriophage MS2. For the experiment, the MS2 protein is fused to the MBP. The fused ncRNA is overexpressed *in vivo* prior to cell lysis. The soluble cellular (lysate) content is then transferred into a column containing an amylose resin added in order to fix the MS2-MBP fusion. Once the lysate is passed through the column, a solution of maltose is used to pull down the MS2-CcnA complexes with RNAs or proteins interacting with CcnA. The identification and characterization of direct *in vivo* partners of CcnA is then made by Western blotting, mass spectrometry, or RNAseq. CcnA, cell cycle noncoding RNA A; MAPS, MS2-affinity purification coupled with RNA sequencing; MBP, maltose binding protein; ncRNA, noncoding RNA; RNAseq, RNA sequencing.
(TIF)

S11 Fig. (**A)** MAPS experiment was performed using an MS2-CcnA construct. Untagged CcnA was used as a control. Cells were grown in PYE at 30˚C until $OD_{600nm} = 0.6$ and harvested after induction of P*lac-ms2-ccnA* and P*lac-ccnA* by addition of IPTG 1 mM 30 min. After pull-down and RNAseq, data were normalized using RPKM method. Mapped reads of *ccnA* locus are visualized by using IGV. (**B)** Same as (A) but here mapped reads of *ctrA* locus are visualized. The highest peak corresponds to a putative interaction site (CcnA in red; 5′ UTR of *ctrA* mRNA in blue). (**C)** Same as (A) but MAPS was performed using MS2-5′ UTRs of *ctrA* generated by promoters *ctrA* P1 (UTR- *P1-ctrA-ms2)* or *ctrA* P2 (UTR- *P2-ctrA -ms2)*. Mapped reads of P1 and P2 5′ UTRs in the vicinity of *ctrA* mRNA were visualized. The red line shows reads corresponding to transcription until 20 amino acids of *ctrA*. (**D)** Same as (C) but here mapped reads in the vicinity of *ccnA* were visualized by using IGV. CcnA, cell cycle noncoding RNA A; IGV, Integrative Genomics Viewer; MAPS, MS2-affinity purification coupled with RNA sequencing; PYE, peptone yeast extract; RNAseq, RNA sequencing; RPKM, reads per kilobase per million mapped reads; 5′ UTR, 5′ untranslated region.
(TIF)

S12 Fig. RNAseq and MAPS data integration. MAPS experiment was performed using an MS2-CcnA construct. Untagged CcnA was used as a control. Cells were grown in PYE at 30˚C until $OD_{600nm} = 0.6$ and harvested after induction of P*lac-ms2-ccnA* and P*lac-ccnA* by addition of IPTG 1 mM 30 min. After pull-down and RNAseq, reads were mapped to the indexed *C. crescentus* NA1000 genome (NC_011916) and mRNAs potentially bound or not to CcnA were identified. In parallel, an additional RNAseq of transcriptome of cells carrying either P*lac-ccnA* or P*lac-ccnA-as* was performed in order to analyze expression profiles of CcnA targets. The figure summarizes the information regarding genes identified as differentially expressed comparing the RNAseq results for strain carrying P*lac-ccnA* (CcnA-sense) and those for strain carrying P*lac-ccnA-as* (CcnA-antisense) (see Materials and methods). On the left heatmap, we show the fold change in the contrast CcnA-sense vs. CcnA-antisense, while on the right, we show the corresponding DESeq2 normalized transcript abundances in the 2 genetic backgrounds (combination of 3 biological replicates each). Several genes of interest (see text for more details) are highlighted in colors: cell cycle factors, including CtrA and GcrA, are in red;

polar and motility genes are in green. Binary (presence of CtrA binding sites, cell cycle dependency, methylation dependency, essentiality) and COG annotations are represented in different colors for clarity; quantitative information (number of GGGG patterns upstream of the gene, enrichment in GcrA ChIP-seq reads, and number of MAPS experiments where the gene was significantly enriched) are colored accordingly to the maps specified at the bottom left. Data sources and methods are detailed in Material and methods. CcnA, cell cycle noncoding RNA A; MAPS, MS2-affinity purification coupled with RNA sequencing; PYE, peptone yeast extract; RNAseq, RNA sequencing.
(TIF)

S13 Fig. Schematic representation of the GcrA-CcrM epigenetic transcriptional regulation of *ctrA-P1*. The expression of *ctrA* depends on the GcrA-CcrM module. CcrM mediates the methylation of the P1 promoter of *ctrA*, recruiting GcrA, which, in turn, activates the transcription of CtrA. In a Δ*ccrM* background, the levels of CtrA are low. However, considering that the *ctrA P1* promoter is sigma70 dependent, transcription of *ctrA* will keep a basal low expression.
(TIF)

S14 Fig. (**A)** Cell curvature of WT cells and Δ*ccrM*+ P*lac-ccnA* from (6A) was determined using MicrobeJ [37]. Approximately 683 cells were analyzed for each condition, and statistical significance was determined using an unpaired *t* test. ****: p.val < 0.0001. The *ΔccrM* and *ΔccrM* + empty vector cells were not considered for this analysis because the filamentous phenotypes observed in these 2 mutants result in cell curvature artifacts measurements that are not consistent with the MicrobeJ analysis. Raw data are provided in S8 Table. (**B)** WT cells, WT cells carrying an empty vector or *Plac-ccnA* were grown in PYE at 30˚C until OD_{600nm} = 0.6. Then, induction of P*lac-ccnA* was made by addition of IPTG 1 mM 30 min. As a control of induction, WT cells carrying an empty vector were also incubated 30 min in presence of IPTG 1 mM and WT cells with no induction were used as a control. (NI = no IPTG) and (I = IPTG). Proteins were extracted and separated on a SDS-PAGE gel for western blotting. GcrA and MreB (loading control) proteins were revealed using specific polyclonal antibodies on nitrocellulose membranes. (**C)** Same as (B) but here proteins from a biological replicate of P*lac-ccnA* cells were extracted and separated on a SDS-PAGE gel for Western blotting. CtrA and MreB (loading control) proteins were revealed using specific polyclonal antibodies on nitrocellulose membranes. (**D)** WT cells, Δ*prom* cells, Δ*prom* cells carrying either a pMR10 low-copy plasmid harboring *ccnA* under the control of its own promoter (Δ*prom* + P*ccnA-ccnA)* or *ccnA*, its antisense under the control of a P*lac* promoter (Δ*prom*+ P*lac-ccnA*, Δ*prom* + P*lac-ccnA-as)* and an empty pSRK used as a control (Δ*prom* + empty vector*)* were grown in PYE at 30˚C until OD_{600nm} = 0.6. For Δ*prom*+ P*lac-ccnA*, Δ*prom* + P*lac-ccnA-as* cells, expression of *ccnA* or its antisense was made by addition of IPTG 1 mM 30 min. As a control, Δ*prom* cells carrying the empty pSRK were also incubated 30 min in presence of IPTG 1 mM 30 min. Proteins were extracted and separated on a SDS-PAGE gel for Western blotting. CtrA and MreB (loading control) proteins were revealed using specific polyclonal antibodies on nitrocellulose membranes. (**E)** INTA RNA analysis on the 5′ UTRs of *ctrA* P2 and *gcrA* using CcnA as bait. For both UTRs, the upper sequence corresponds to the target gene sequence while CcnA is in the lower sequence. PYE, peptone yeast extract; WT, wild-type.
(TIF)

S15 Fig. Δ*pleC*+ P*lac-ccnA* or Δ*pleC*+ P*lac-ccnA-as* were grown in PYE at 30˚C until OD_{600nm} = 0.6. Then, induction of P*lac-ccnA* and *Plac-ccnA-as* was made by addition of IPTG 1 mM 30 min. In parallel, as a control, Δ*pleC* cells were grown in PYE at 30˚C until OD_{600nm} = 0.6 and

harvested. Proteins were extracted and separated on a SDS-PAGE gel containing Phostag and Mn^{2+} to visualize CtrA phosphorylation level. As a Phostag control, an additional sample of Δ*pleC* cells pellet was boiled 10 min in order to discriminate the migration on the gel of the CtrA phosphorylated band from the nonphosphorylated band. CtrA was revealed using specific polyclonal antibodies on nitrocellulose membranes. PYE, peptone yeast extract.
(TIF)

S16 Fig. (**A**) Phase contrast images of *S. meliloti* WT cells, carrying either an empty pSRK (empty vector) or *ccnA* under the control of a P*lac* promoter (P*lac-ccnA)* from *C. crescentus* were grown in TY at 30˚C until OD_{600nm} = 0.6. (**B**) WT *S. meliloti* carrying either an empty vector or P*lac-ccnA* were grown in TY at 30˚C until OD_{600nm} = 0.6. Then, the induction of P*lac-ccnA* was made by addition of IPTG 1 mM 30 min. Proteins were extracted and separated on a SDS-PAGE gel for Western blotting. CtrA and GroEL (loading control) proteins were revealed using specific polyclonal antibodies on a nitrocellulose membrane. (**C**) Putative homologs of *ccnA* in the class *Alphaproteobacteria*. Research of homologs was performed using the online sRNA Homolog Finder GlassGo [93] using *C. crescentus ccnA* sequence as query. The heatmap contains identity percentages shared by CcnA homologs in different species and was then transformed into a distance matrix to build the dendrogram on the top. Comparisons were done in pairs because a multiple alignment of all CcnA homologs contains too many gaps. Data are in S9 Table. (**D**) ClustalOmega [94,95] alignment of 5′ UTRs of *ctrA* from *S. meliloti* and *C. crescentus* starting from GGGG (red) motif near the start codon ATG (green) until nucleotide +25. Clustal Omega was used with default parameters for RNA. "*" represents a conserved nucleotide between the 2 sequences. TY, tryptone-yeast; WT, wild-type.
(TIF)

Acknowledgments

We thank members of the Biondi and Massé's laboratory for critical comments on the manuscript. We thank the IMM Transcriptomic facility for the RNA preparation and the qRT-PCR experiment; we also thank Artemis Kosta and Hugo le Guenno from the IMM Microscopy platform for Electron Microscopy acquisition and analysis. We thank also Gaël Panis and Patrick Viollier for the phage CbK and also for providing the delta *cpdR*, *rcdA*, *popA* strains used in this work. We thank Regis Hallez and Romain Mercier for MreB and GFP antibodies, respectively, used in this study.

Author Contributions

Conceptualization: Marta Robledo Garrido, Jose-Ignacio Jimenez-Zurdo, Eric Massé, Emanuele G. Biondi.

Data curation: Wanassa Beroual, David Lalaouna, Yann Denis, Gaël Brasseur, Matteo Brilli, Emanuele G. Biondi.

Formal analysis: Wanassa Beroual, Karine Prévost, David Lalaouna, Meriem Djendli, Matteo Brilli.

Funding acquisition: Emanuele G. Biondi.

Investigation: Wanassa Beroual, Karine Prévost, David Lalaouna, Nadia Ben Zaina, Odile Valette, Yann Denis, Gaël Brasseur, Matteo Brilli, Marta Robledo Garrido, Jose-Ignacio Jimenez-Zurdo, Eric Massé.

Methodology: Wanassa Beroual, Karine Prévost, David Lalaouna, Nadia Ben Zaina, Odile Valette, Yann Denis, Gaël Brasseur, Matteo Brilli, Eric Massé.

Project administration: Emanuele G. Biondi.

Supervision: Emanuele G. Biondi.

Validation: Emanuele G. Biondi.

Writing – original draft: Emanuele G. Biondi.

Writing – review & editing: Wanassa Beroual, Matteo Brilli, Eric Massé.

References

1. Collier J. Regulation of chromosomal replication in Caulobacter crescentus. Plasmid. 2012; 67:76–87. https://doi.org/10.1016/j.plasmid.2011.12.007 PMID: 22227374
2. Skerker JM, Laub MT. Cell-cycle progression and the generation of asymmetry in Caulobacter crescentus. Nat Rev Microbiol. 2004; 2:325–37. https://doi.org/10.1038/nrmicro864 PMID: 15031731
3. Collier J, Murray SR, Shapiro L. DnaA couples DNA replication and the expression of two cell cycle master regulators. EMBO J. 2006; 25:346–56. https://doi.org/10.1038/sj.emboj.7600927 PMID: 16395331
4. Collier J, McAdams HH, Shapiro L. A DNA methylation ratchet governs progression through a bacterial cell cycle. Proc Natl Acad Sci U S A. 2007; 104:17111–6. https://doi.org/10.1073/pnas.0708112104 PMID: 17942674
5. Reisenauer A, Shapiro L. DNA methylation affects the cell cycle transcription of the CtrA global regulator in Caulobacter. EMBO J. 2002; 21:4969–77. https://doi.org/10.1093/emboj/cdf490 PMID: 12234936
6. Panis G, Murray SR, Viollier PH. Versatility of global transcriptional regulators in alpha-Proteobacteria: from essential cell cycle control to ancillary functions. FEMS Microbiol Rev. 2015; 39:120–33. https://doi.org/10.1093/femsre/fuu002 PMID: 25793963
7. Delaby M, Panis G, Viollier PH. Bacterial cell cycle and growth phase switch by the essential transcriptional regulator CtrA. Nucleic Acids Res. 2019; 47:10628–44. https://doi.org/10.1093/nar/gkz846 PMID: 31598724
8. Fumeaux C, Radhakrishnan SK, Ardissone S, Théraulaz L, Frandi A, Martins D, et al. Cell cycle transition from S-phase to G1 in Caulobacter is mediated by ancestral virulence regulators. Nat Commun. 2014; 5:4081. https://doi.org/10.1038/ncomms5081 PMID: 24939058
9. Gora KG, Tsokos CG, Chen YE, Srinivasan BS, Perchuk BS, Laub MT. A cell-type-specific protein-protein interaction modulates transcriptional activity of a master regulator in Caulobacter crescentus. Mol Cell. 2010; 39:455–67. https://doi.org/10.1016/j.molcel.2010.06.024 PMID: 20598601
10. Gora KG, Cantin A, Wohlever M, Joshi KK, Perchuk BS, Chien P, et al. Regulated proteolysis of a transcription factor complex is critical to cell cycle progression in Caulobacter crescentus. Mol Microbiol. 2013; 87:1277–89. https://doi.org/10.1111/mmi.12166 PMID: 23368090
11. Laub MT, Chen SL, Shapiro L, McAdams HH. Genes directly controlled by CtrA, a master regulator of the Caulobacter cell cycle. Proc Natl Acad Sci U S A. 2002; 99:4632–7. https://doi.org/10.1073/pnas.062065699 PMID: 11930012
12. Marczynski GT, Shapiro L. Control of chromosome replication in caulobacter crescentus. Annu Rev Microbiol. 2002; 56:625–56. https://doi.org/10.1146/annurev.micro.56.012302.161103 PMID: 12142494
13. Quon KC, Yang B, Domian IJ, Shapiro L, Marczynski GT. Negative control of bacterial DNA replication by a cell cycle regulatory protein that binds at the chromosome origin. Proc Natl Acad Sci U S A. 1998; 95:120–5. https://doi.org/10.1073/pnas.95.1.120 PMID: 9419339
14. Fioravanti A, Fumeaux C, Mohapatra SS, Bompard C, Brilli M, Frandi A, et al. DNA Binding of the Cell Cycle Transcriptional Regulator GcrA Depends on N6-Adenosine Methylation in Caulobacter crescentus and Other Alphaproteobacteria. PLoS Genet. 2013; 9:e1003541. https://doi.org/10.1371/journal.pgen.1003541 PMID: 23737758
15. Haakonsen DL, Yuan AH, Laub MT. The bacterial cell cycle regulator GcrA is a σ70 cofactor that drives gene expression from a subset of methylated promoters. Genes Dev. 2015; 29:2272–86. https://doi.org/10.1101/gad.270660.115 PMID: 26545812

16. Holtzendorff J, Hung D, Brende P, Reisenauer A, Viollier PH, McAdams HH, et al. Oscillating global regulators control the genetic circuit driving a bacterial cell cycle. Science. 2004; 304:983–7. https://doi.org/10.1126/science.1095191 PMID: 15087506

17. Mohapatra SS, Fioravanti A, Vandame P, Spriet C, Pini F, Bompard C, et al. Methylation-dependent transcriptional regulation of crescentin gene (creS) by GcrA in Caulobacter crescentus. Mol Microbiol. 2020. https://doi.org/10.1111/mmi.14500 PMID: 32187735

18. Biondi EG, Reisinger SJ, Skerker JM, Arif M, Perchuk BS, Ryan KR, et al. Regulation of the bacterial cell cycle by an integrated genetic circuit. Nature. 2006; 444:899–904. https://doi.org/10.1038/nature05321 PMID: 17136100

19. Chen YE, Tropini C, Jonas K, Tsokos CG, Huang KC, Laub MT. Spatial gradient of protein phosphorylation underlies replicative asymmetry in a bacterium. Proc Natl Acad Sci U S A. 2011; 108:1052–7. https://doi.org/10.1073/pnas.1015397108 PMID: 21191097

20. Jacobs C, Ausmees N, Cordwell SJ, Shapiro L, Laub MT. Functions of the CckA histidine kinase in Caulobacter cell cycle control. Mol Microbiol. 2003; 47:1279–90. https://doi.org/10.1046/j.1365-2958.2003.03379.x PMID: 12603734

21. Joshi KK, Bergé M, Radhakrishnan SK, Viollier PH, Chien P. An Adaptor Hierarchy Regulates Proteolysis during a Bacterial Cell Cycle. Cell. 2015; 163:419–31. https://doi.org/10.1016/j.cell.2015.09.030 PMID: 26451486

22. Ryan KR, Huntwork S, Shapiro L. Recruitment of a cytoplasmic response regulator to the cell pole is linked to its cell cycle-regulated proteolysis. Proc Natl Acad Sci U S A. 2004; 101:7415–20. https://doi.org/10.1073/pnas.0402153101 PMID: 15123835

23. Keiler KC, Shapiro L. tmRNA Is Required for Correct Timing of DNA Replication in Caulobacter crescentus. J Bacteriol. 2003; 185:573–80. https://doi.org/10.1128/JB.185.2.573-580.2003 PMID: 12511504

24. Wurihan W, Wunier W, Li H, Fan LF, Morigen M. Trans-translation ensures timely initiation of DNA replication and DnaA synthesis in Escherichia coli. Genet Mol Res. 2016;15. https://doi.org/10.4238/gmr.15038407 PMID: 27706629

25. Landt SG, Abeliuk E, McGrath PT, Lesley JA, McAdams HH, Shapiro L. Small non-coding RNAs in Caulobacter crescentus. Mol Microbiol. 2008; 68:600–14. https://doi.org/10.1111/j.1365-2958.2008.06172.x PMID: 18373523

26. Landt SG, Lesley JA, Britos L, Shapiro L. CrfA, a small noncoding RNA regulator of adaptation to carbon starvation in Caulobacter crescentus. J Bacteriol. 2010; 192:4763–75. https://doi.org/10.1128/JB.00343-10 PMID: 20601471

27. Tien M, Fiebig A, Crosson S. Gene network analysis identifies a central post-transcriptional regulator of cellular stress survival. elife. 2018;7. https://doi.org/10.7554/eLife.33684 PMID: 29537368

28. Fröhlich KS, Förstner KU, Gitai Z. Post-transcriptional gene regulation by an Hfq-independent small RNA in Caulobacter crescentus. Nucleic Acids Res. 2018; 46:10969–82. https://doi.org/10.1093/nar/gky765 PMID: 30165530

29. Beroual W, Brilli M, Biondi EG. Non-coding RNAs Potentially Controlling Cell Cycle in the Model Caulobacter crescentus: A Bioinformatic Approach. Front Genet. 2018; 9:164. https://doi.org/10.3389/fgene.2018.00164 PMID: 29899753

30. Levine E, Zhang Z, Kuhlman T, Hwa T. Quantitative characteristics of gene regulation by small RNA. PLoS Biol. 2007; 5:e229. https://doi.org/10.1371/journal.pbio.0050229 PMID: 17713988

31. Mitarai N, Benjamin J-AM, Krishna S, Semsey S, Csiszovszki Z, Massé E, et al. Dynamic features of gene expression control by small regulatory RNAs. Proc Natl Acad Sci U S A. 2009; 106:10655–9. https://doi.org/10.1073/pnas.0901466106 PMID: 19541626

32. Zhou B, Schrader JM, Kalogeraki VS, Abeliuk E, Dinh CB, Pham JQ, et al. The global regulatory architecture of transcription during the Caulobacter cell cycle. PLoS Genet. 2015; 11:e1004831. https://doi.org/10.1371/journal.pgen.1004831 PMID: 25569173

33. Brilli M, Fondi M, Fani R, Mengoni A, Ferri L, Bazzicalupo M, et al. The diversity and evolution of cell cycle regulation in alpha-proteobacteria: a comparative genomic analysis. BMC Syst Biol. 2010; 4:52. https://doi.org/10.1186/1752-0509-4-52 PMID: 20426835

34. Quon KC, Marczynski GT, Shapiro L. Cell cycle control by an essential bacterial two-component signal transduction protein. Cell. 1996; 84:83–93. https://doi.org/10.1016/s0092-8674(00)80995-2 PMID: 8548829

35. Siam R, Brassinga AKC, Marczynski GT. A dual binding site for integration host factor and the response regulator CtrA inside the Caulobacter crescentus replication origin. J Bacteriol. 2003; 185:5563–72. https://doi.org/10.1128/JB.185.18.5563-5572.2003 PMID: 12949109

36. Khan SR, Gaines J, Roop RM 2nd, Farrand SK. Broad-host-range expression vectors with tightly regulated promoters and their use to examine the influence of TraR and TraM expression on Ti plasmid quorum sensing. Appl Environ Microbiol. 2008; 74:5053–62. https://doi.org/10.1128/AEM.01098-08 PMID: 18606801

37. Ducret A, Quardokus EM, Brun YV. MicrobeJ, a tool for high throughput bacterial cell detection and quantitative analysis. Nat Microbiol. 2016; 1:16077. https://doi.org/10.1038/nmicrobiol.2016.77 PMID: 27572972

38. Biondi EG, Skerker JM, Arif M, Prasol MS, Perchuk BS, Laub MT. A phosphorelay system controls stalk biogenesis during cell cycle progression in Caulobacter crescentus. Mol Microbiol. 2006; 59:386–401. https://doi.org/10.1111/j.1365-2958.2005.04970.x PMID: 16390437

39. McGrath PT, Iniesta AA, Ryan KR, Shapiro L, McAdams HH. A dynamically localized protease complex and a polar specificity factor control a cell cycle master regulator. Cell. 2006; 124:535–47. https://doi.org/10.1016/j.cell.2005.12.033 PMID: 16469700

40. Pini F, Frage B, Ferri L, De Nisco NJ, Mohapatra SS, Taddei L, et al. The DivJ, CbrA and PleC system controls DivK phosphorylation and symbiosis in Sinorhizobium meliloti. Mol Microbiol. 2013; 90:54–71. https://doi.org/10.1111/mmi.12347 PMID: 23909720

41. Christen B, Abeliuk E, Collier JM, Kalogeraki VS, Passarelli B, Coller JA, et al. The essential genome of a bacterium. Mol Syst Biol. 2011; 7:528. https://doi.org/10.1038/msb.2011.58 PMID: 21878915

42. Taylor JA, Ouimet M-C, Wargachuk R, Marczynski GT. The Caulobacter crescentus chromosome replication origin evolved two classes of weak DnaA binding sites. Mol Microbiol. 2011; 82:312–26. https://doi.org/10.1111/j.1365-2958.2011.07785.x PMID: 21843309

43. Skerker JM, Prasol MS, Perchuk BS, Biondi EG, Laub MT. Two-component signal transduction pathways regulating growth and cell cycle progression in a bacterium: a system-level analysis. PLoS Biol. 2005; 3:e334. https://doi.org/10.1371/journal.pbio.0030334 PMID: 16176121

44. Frandi A, Collier J. Multilayered control of chromosome replication in Caulobacter crescentus. Biochem Soc Trans. 2019; 47:187–96. https://doi.org/10.1042/BST20180460 PMID: 30626709

45. Marczynski GT, Lentine K, Shapiro L. A developmentally regulated chromosomal origin of replication uses essential transcription elements. Genes Dev. 1995; 9:1543–57. https://doi.org/10.1101/gad.9.12.1543 PMID: 7601356

46. Lalaouna D, Carrier M-C, Semsey S, Brouard J-S, Wang J, Wade JT, et al. A 3' external transcribed spacer in a tRNA transcript acts as a sponge for small RNAs to prevent transcriptional noise. Mol Cell. 2015; 58:393–405. https://doi.org/10.1016/j.molcel.2015.03.013 PMID: 25891076

47. Mann M, Wright PR, Backofen R. IntaRNA 2.0: enhanced and customizable prediction of RNA–RNA interactions. Nucleic Acids Res. 2017; 45:W435–9. https://doi.org/10.1093/nar/gkx279 PMID: 28472523

48. Zuker M. Mfold web server for nucleic acid folding and hybridization prediction. Nucleic Acids Res. 2003; 31:3406–15. https://doi.org/10.1093/nar/gkg595 PMID: 12824337

49. Gonzalez D, Collier J. DNA methylation by CcrM activates the transcription of two genes required for the division of Caulobacter crescentus. Mol Microbiol. 2013; 88:203–18. https://doi.org/10.1111/mmi.12180 PMID: 23480529

50. Fang G, Passalacqua KD, Hocking J, Llopis PM, Gerstein M, Bergman NH, et al. Transcriptomic and phylogenetic analysis of a bacterial cell cycle reveals strong associations between gene co-expression and evolution. BMC Genomics. 2013; 14:450. https://doi.org/10.1186/1471-2164-14-450 PMID: 23829427

51. Eraso JM, Markillie LM, Mitchell HD, Taylor RC, Orr G, Margolin W. The highly conserved MraZ protein is a transcriptional regulator in Escherichia coli. J Bacteriol. 2014; 196:2053–66. https://doi.org/10.1128/JB.01370-13 PMID: 24659771

52. Alyahya SA, Alexander R, Costa T, Henriques AO, Emonet T, Jacobs-Wagner C. RodZ, a component of the bacterial core morphogenic apparatus. Proc Natl Acad Sci. 2009; 106:1239–44. https://doi.org/10.1073/pnas.0810794106 PMID: 19164570

53. de Araújo HL, Martins BP, Vicente AM, Lorenzetti APR, Koide T, Marques MV. Cold Regulation of Genes Encoding Ion Transport Systems in the Oligotrophic Bacterium Caulobacter crescentus. Gralnick JA, editor. Microbiol Spectr. 2021;9. https://doi.org/10.1128/Spectrum.00710-21 PMID: 34479415

54. Mazzon RR, Lang EAS, Silva CAPT, Marques MV. Cold Shock Genes cspA and cspB from Caulobacter crescentus Are Posttranscriptionally Regulated and Important for Cold Adaptation. J Bacteriol. 2012; 194:6507–17. https://doi.org/10.1128/JB.01422-12 PMID: 23002229

55. Murray SM, Panis G, Fumeaux C, Viollier PH, Howard M. Computational and genetic reduction of a cell cycle to its simplest, primordial components. PLoS Biol. 2013; 11:e1001749. https://doi.org/10.1371/journal.pbio.1001749 PMID: 24415923

56. Panis G, Lambert C, Viollier PH. Complete genome sequence of Caulobacter crescentus bacteriophage φCbK. J Virol. 2012; 86:10234–5. https://doi.org/10.1128/JVI.01579-12 PMID: 22923796

57. Sommer JM, Newton A. Sequential regulation of developmental events during polar morphogenesis in Caulobacter crescentus: assembly of pili on swarmer cells requires cell separation. J Bacteriol. 1988; 170:409–15. https://doi.org/10.1128/jb.170.1.409-415.1988 PMID: 2891681

58. Coppine J, Kaczmarczyk A, Petit K, Brochier T, Jenal U, Hallez R. Regulation of Bacterial Cell Cycle Progression by Redundant Phosphatases. J Bacteriol. 2020; 202:e00345–20. https://doi.org/10.1128/JB.00345-20 PMID: 32571969

59. Hartmann R, Teeseling MCF, Thanbichler M, Drescher K. BacStalk: A comprehensive and interactive image analysis software tool for bacterial cell biology. Mol Microbiol 2020; 114: 140–150. https://doi.org/10.1111/mmi.14501 PMID: 32190923

60. Pini F, De Nisco NJ, Ferri L, Penterman J, Fioravanti A, Brilli M, et al. Cell Cycle Control by the Master Regulator CtrA in Sinorhizobium meliloti. PLoS Genet. 2015; 11:e1005232. https://doi.org/10.1371/journal.pgen.1005232 PMID: 25978424

61. Lott SC, Schäfer RA, Mann M, Backofen R, Hess WR, Voß B, et al. GLASSgo–Automated and Reliable Detection of sRNA Homologs From a Single Input Sequence. Front Genet. 2018;9. https://doi.org/10.3389/fgene.2018.00009 PMID: 29472945

62. Schrader JM, Zhou B, Li G-W, Lasker K, Childers WS, Williams B, et al. The coding and noncoding architecture of the Caulobacter crescentus genome. PLoS Genet. 2014; 10:e1004463. https://doi.org/10.1371/journal.pgen.1004463 PMID: 25078267

63. Zhan Y, Yan Y, Deng Z, Chen M, Lu W, Lu C, et al. The novel regulatory ncRNA, NfiS, optimizes nitrogen fixation via base pairing with the nitrogenase gene nifK mRNA in Pseudomonas stutzeri A1501. Proc Natl Acad Sci U S A. 2016; 113:E4348–56. https://doi.org/10.1073/pnas.1604514113 PMID: 27407147

64. Jagodnik J, Chiaruttini C, Guillier M. Stem-Loop Structures within mRNA Coding Sequences Activate Translation Initiation and Mediate Control by Small Regulatory RNAs. Mol Cell. 2017; 68:158–170.e3. https://doi.org/10.1016/j.molcel.2017.08.015 PMID: 28918899

65. Markham NR, Zuker M. DINAMelt web server for nucleic acid melting prediction. Nucleic Acids Res. 2005; 33:W577–81. https://doi.org/10.1093/nar/gki591 PMID: 15980540

66. Kaczmarczyk A, Hempel AM, von Arx C, Böhm R, Dubey BN, Nesper J, et al. Precise timing of transcription by c-di-GMP coordinates cell cycle and morphogenesis in Caulobacter. Nat Commun. 2020; 11:816. https://doi.org/10.1038/s41467-020-14585-6 PMID: 32041947

67. Dutta T, Srivastava S. Small RNA-mediated regulation in bacteria: A growing palette of diverse mechanisms. Gene. 2018. https://doi.org/10.1016/j.gene.2018.02.068 PMID: 29501814

68. Mandin P, Guillier M. Expanding control in bacteria: interplay between small RNAs and transcriptional regulators to control gene expression. Curr Opin Microbiol. 2013; 16:125–32. https://doi.org/10.1016/j.mib.2012.12.005 PMID: 23415757

69. Nitzan M, Rehani R, Margalit H. Integration of Bacterial Small RNAs in Regulatory Networks. Annu Rev Biophys. 2017; 46:131–48. https://doi.org/10.1146/annurev-biophys-070816-034058 PMID: 28532217

70. Liu D, Chang X, Liu Z, Chen L, Wang R. Bistability and oscillations in gene regulation mediated by small noncoding RNAs. PLoS ONE. 2011; 6:e17029. https://doi.org/10.1371/journal.pone.0017029 PMID: 21437279

71. Greene SE, Brilli M, Biondi EG, Komeili A. Analysis of the CtrA pathway in Magnetospirillum reveals an ancestral role in motility in alphaproteobacteria. J Bacteriol. 2012; 194:2973–86. https://doi.org/10.1128/JB.00170-12 PMID: 22467786

72. Marks ME, Castro-Rojas CM, Teiling C, Du L, Kapatral V, Walunas TL, et al. The genetic basis of laboratory adaptation in Caulobacter crescentus. J Bacteriol. 2010; 192:3678–88. https://doi.org/10.1128/JB.00255-10 PMID: 20472802

73. Schneider CA, Rasband WS, Eliceiri KW. NIH Image to ImageJ: 25 years of image analysis. Nat Methods. 2012; 9:671–5. https://doi.org/10.1038/nmeth.2089 PMID: 22930834

74. Lalaouna D, Prévost K, Eyraud A, Massé E. Identification of unknown RNA partners using MAPS. Methods. 2017; 117:28–34. https://doi.org/10.1016/j.ymeth.2016.11.011 PMID: 27876680

75. Hartmann R, Teeseling MCF, van Thanbichler M, Drescher K. BacStalk: A comprehensive and interactive image analysis software tool for bacterial cell biology. Mol Microbiol. https://doi.org/10.1111/mmi.14501 PMID: 32190923

76. Afgan E, Baker D, van den Beek M, Blankenberg D, Bouvier D, Čech M, et al. The Galaxy platform for accessible, reproducible and collaborative biomedical analyses: 2016 update. Nucleic Acids Res. 2016; 44:W3 –W10. https://doi.org/10.1093/nar/gkw343 PMID: 27137889

77. Ramírez F, Dündar F, Diehl S, Grüning BA, Manke T. deepTools: a flexible platform for exploring deep-sequencing data. Nucleic Acids Res. 2014; 42:W187–91. https://doi.org/10.1093/nar/gku365 PMID: 24799436

78. Robinson JT, Thorvaldsdóttir H, Winckler W, Guttman M, Lander ES, Getz G, et al. Integrative genomics viewer. Nat Biotechnol. 2011; 29:24–6. https://doi.org/10.1038/nbt.1754 PMID: 21221095

79. Langmead B, Salzberg SL, Slazberg SL. Fast gapped-read alignment with Bowtie 2. Nat Methods. 2012; 9:357–9. https://doi.org/10.1038/nmeth.1923 PMID: 22388286

80. Li H, Handsaker B, Wysoker A, Fennell T, Ruan J, Homer N, et al. The Sequence Alignment/Map format and SAMtools. Bioinformatics. 2009; 25:2078–9. https://doi.org/10.1093/bioinformatics/btp352 PMID: 19505943

81. Anders S, Pyl PT, Huber W. HTSeq-A Python framework to work with high-throughput sequencing data. Bioinformatics. 2015; 31:166–9. https://doi.org/10.1093/bioinformatics/btu638 PMID: 25260700

82. Love MI, Huber W, Anders S. Moderated estimation of fold change and dispersion for RNA-seq data with DESeq2. Genome Biol. 2014; 15:550. https://doi.org/10.1186/s13059-014-0550-8 PMID: 25516281

83. Christen B, Abeliuk E, Collier JM, Kalogeraki VS, Passarelli B, Coller JA, et al. The essential genome of a bacterium. Mol Syst Biol. 2011; 7:1–7. https://doi.org/10.1038/msb.2011.58 PMID: 21878915

84. Fang G, Passalacqua KD, Hocking J, Llopis PM, Gerstein MB, Bergman NH, et al. Transcriptomic and phylogenetic analysis of a bacterial cell cycle reveals strong associations between gene co-expression and evolution. BMC Genomics. 2013; 14:450. https://doi.org/10.1186/1471-2164-14-450 PMID: 23829427

85. Haakonsen DL, Yuan AH, Laub MT. The bacterial cell cycle regulator GcrA is a $σ$ 70 cofactor that drives gene expression from a subset of methylated promoters. Genes Dev. 2015; 29:2272–86. https://doi.org/10.1101/gad.270660.115 PMID: 26545812

86. Gonzalez D, Kozdon JB, Mcadams HH, Shapiro L, Collier J. The functions of DNA methylation by CcrM in Caulobacter crescentus: A global approach. Nucleic Acids Res. 2014; 42:3720–35. https://doi.org/10.1093/nar/gkt1352 PMID: 24398711

87. Brilli M, Fondi M, Fani R, Mengoni A, Ferri L, Bazzicalupo M, et al. The diversity and evolution of cell cycle regulation in alpha-proteobacteria: A comparative genomic analysis. BMC Syst Biol. 2010;4. https://doi.org/10.1186/1752-0509-4-4 PMID: 20100324

88. Beroual W, Biondi EG. The non-coding RNA CcnA modulates the master cell cycle regulators CtrA and GcrA in Caulobacter crescentus. 2022. Dryad Digital Repository. Openly available via: https://doi.org/10.1016/j.scitotenv.2021.152861 PMID: 34998768

89. Morita T, Maki K, Aiba H. Detection of sRNA-mRNA interactions by electrophoretic mobility shift assay. Methods Mol Biol. 2012; 905:235–44. https://doi.org/10.1007/978-1-61779-949-5_15 PMID: 22736008

90. McClure R, Balasubramanian D, Sun Y, Bobrovskyy M, Sumby P, Genco CA, et al. Computational analysis of bacterial RNA-Seq data. Nucleic Acids Res. 2013; 41:e140. https://doi.org/10.1093/nar/gkt444 PMID: 23716638

91. De TB. novo assembly of bacterial transcriptomes from RNA-seq data. Genome Biol. 2015; 16:1. https://doi.org/10.1186/s13059-014-0572-2 PMID: 25583448

92. Ducret A, Quardokus EM, Brun YV. MicrobeJ, a tool for high throughput bacterial cell detection and quantitative analysis. Nat Microbiol. 2016; 1:16077. https://doi.org/10.1038/nmicrobiol.2016.77 PMID: 27572972

93. Lott SC, Schäfer RA, Mann M, Backofen R, Hess WR, Voß B, et al. GLASSgo–Automated and Reliable Detection of sRNA Homologs From a Single Input Sequence. Front Genet. 2018;9. https://doi.org/10.3389/fgene.2018.00009 PMID: 29472945

94. Madeira F, Park Y mi, Lee J, Buso N, Gur T, Madhusoodanan N, et al. The EMBL-EBI search and sequence analysis tools APIs in 2019. Nucleic Acids Res. 2019; 47:W636–41. https://doi.org/10.1093/nar/gkz268 PMID: 30976793

95. Sievers F, Wilm A, Dineen D, Gibson TJ, Karplus K, Li W, et al. Fast, scalable generation of high-quality protein multiple sequence alignments using Clustal Omega. Mol Syst Biol. 2011; 7:539. https://doi.org/10.1038/msb.2011.75 PMID: 21988835